GEOMETRIC ERROR EVALUATION OF PRESSURE AND SUCTION SIDES OF AIRFOIL SECTIONS

by

Rashmi Bhadauria

B.Tech., Motilal Nehru National Institute of Technology, India, 2006

A THESIS SUBMITTED IN PARTIAL FULFILLMENT OF

THE REQUIREMENTS FOR THE DEGREE OF

MASTER OF APPLIED SCIENCE

in

THE FACULTY OF GRADUATE STUDIES

(Mechanical Engineering)

THE UNIVERSITY OF BRITISH COLUMBIA

(Vancouver)

December 2011

Abstract

This thesis presents geometric computing algorithms for the evaluation of geometric errors on the pressure and suction sides of an airfoil section. Airfoil blades such as those in an impeller have a complex freeform geometry which poses significant challenges to the geometric error evaluation tasks. Reliable error evaluation is critical to the impellers as wrongful rejections will lead to significant financial losses. In practice, touch-probe coordinate measuring machines are employed to acquire measurement data points on the impeller blade surface along pre-specified sections. The measurement data points are then used to evaluate against the specified geometric tolerances including the profile tolerance and airfoil thickness control.

Profile tolerances can be defined in three ways: bilateral asymmetric, bilateral symmetric, and unilateral. Existing methods for profile error evaluation are not capable of evaluating all three possible types of profile tolerance. These methods are not adaptive with respect to the specified tolerance zone boundaries. This thesis proposes a novel Scaled Minimax Method which is able to address all types of profile tolerance. The proposed method builds on the conventional Minimax Method and utilizes a scaling constant to control the relative positioning of the evaluated profile error zone boundaries. Thickness control is a less-known tolerance specification for airfoil sections. It controls the overall shape deviation of an airfoil section between the pressure and suction sides. The proposed evaluation method is based on determining a minimum error zone via simultaneously shrinking the outer boundary and growing the inner boundary for the involved measurement data points. Numerous case studies have been performed to validate the effectiveness of the proposed geometric error evaluation methods.

Table of Contents

List of Tables

List of Figures

Acknowledgements

First and foremost, I would like to express my thanks and gratitude to my supervisor Prof. Hsi-Yung (Steve) Feng for giving me the opportunity to study at the University of British Columbia. It has been my privilege to conduct this research under his supervision and I am thankful for his constant support, guidance, and knowledge which he shared during our research meetings.

I would like to thank my family for their unconditional love, constant support, and immense confidence in me over the years.

I would also like to thank the members of the UBC CAD/CAM/CAI Research Laboratory for their support, discussions and friendship.

To My Parents

1 Introduction

Tolerance is an important parameter for the design and manufacturing of components in industry, as it directly impacts the functionality and the production cost of a component. Tolerance is defined as the acceptable deviation from the nominal geometry. Tolerance particularly becomes significant for freeform objects such as impeller and turbines, as they have complex shapes which are difficult to manufacture. Therefore, a robust inspection process is required so that wrongful rejection of the impellers and turbines can be avoided to reduce the wastage of money and other resources.

The subsequent sections in this chapter further elaborate on the importance of tolerance in manufacturing and design, and the inspection techniques adopted in industry. The chapter further focuses on the inspection of impeller blades, their geometry and the associated tolerances. To understand the current research status, a literature review is summarized followed by a statement on the objective of research work in this thesis.

1.1 Importance of tolerance in design and manufacturing

Assignment of tolerances concerns both the design and the manufacturing. Tighter tolerance signifies better quality but may result in excessive manufacturing costs, while loose tolerance may result in bad quality of components and their possible scrap. Figure 1.1 depicts a typical manufacturing cost vs. tolerance relationship. The figure indicates that as the specified tolerance zone gets bigger, the manufacturing cost decreases [1].

Figure 1.2 describes the role of tolerance as a critical link between design and manufacturing. Components are designed in accordance with performance parameters. However,

manufacturing processes cannot produce an exact copy of design. Hence, a certain allowable tolerance which does not hamper the performance of component is assigned on the component. To meet the functional requirements closely, tighter tolerances are always desired in design. On the other hand, manufacturing requires loose tolerance so that it can ease the manufacturing process and lower the production cost in terms of machine tool, fixtures and process selection etc. Optimal tolerances are desired on geometric components to meet the competitive requirements of design and manufacturing [2].
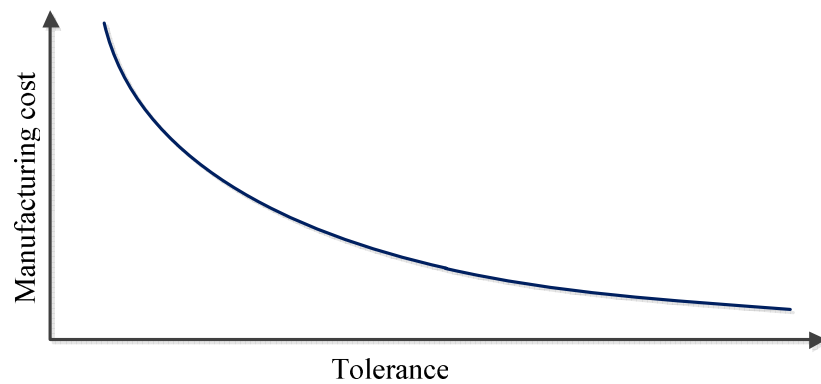
Figure 1.1: Manufacturing cost vs. Tolerance [1]
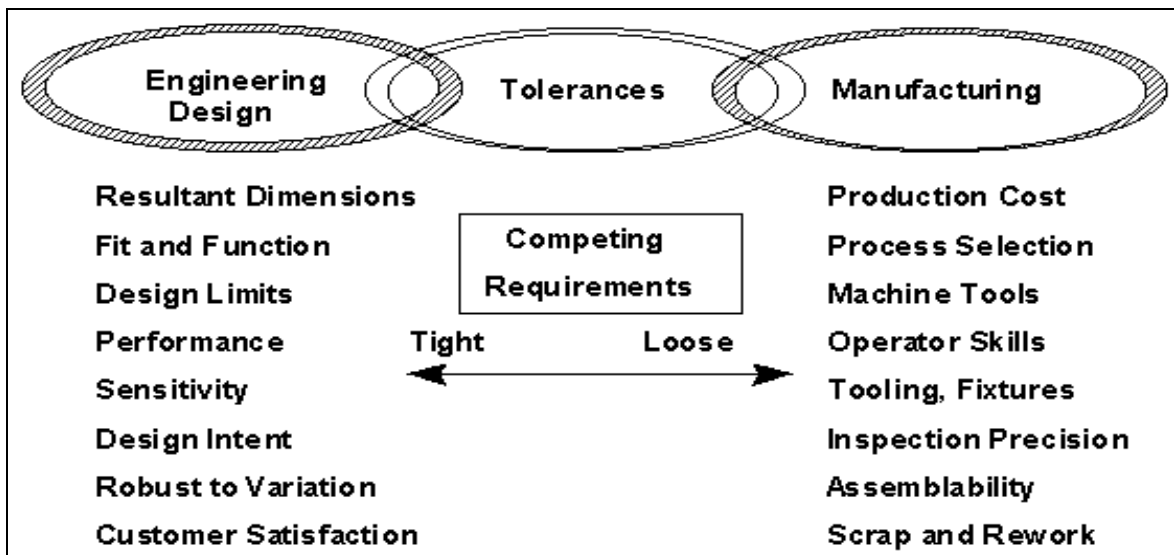
Figure 1.2: Tolerance as a link between engineering design and manufacturing [2]

2

1.2   Computer aided inspection

In order to determine whether specified tolerance is met or not on the manufactured part, inspection needs to be carried out. During inspection, comparison between the manufactured product and the design copy is performed. There are two general approaches for this comparison: direct comparison and indirect comparison. The basic idea of direct comparison is to compare the manufactured part physically with a master template for determining the deviation. For example, as shown in Figure 1.3 for a turbine blade, a master template is prepared for the key cross sections along the blade. The actual blade is then physically kept with this master and gaps are either determined by using a measuring microscope, by dyeing the surface blue or by using a concentrated source of light. The key disadvantages of this method are that it is very slow in nature and depends largely on the inspector. Hence, there is an inconsistency in the results [3].
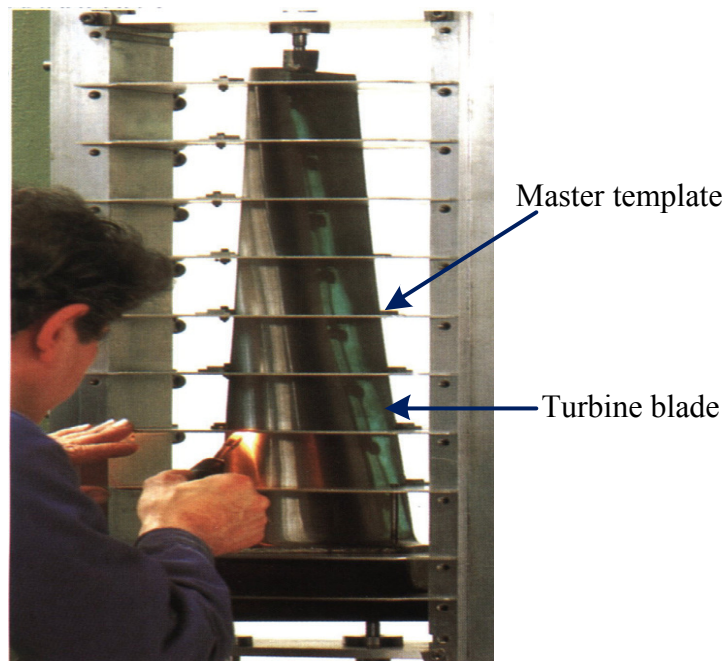
Figure 1.3: Direct comparison of turbine blades with master templates for quality inspection [3]

In indirect comparison, the measurement data points are acquired on the manufactured surface using computer aided machines which are commonly known as coordinate measurement

machines (CMM). The data points are further compared with the design CAD model to evaluate the parameters and geometric tolerances. The measurement can be performed on-line or offline, depending on the requirement of manufacturing process. For on-line gauging, a probe is installed on one of the tool holders of the automatic tool changer. This enables the measurement of the component on the machine itself and if required, correction can be made in the machining parameters as the part is being machined. In the offline inspection method, after manufacturing, the component is taken to a CMM and is inspected separately [3]. CMMs can be broadly classified in to two types depending on the method of data acquisition. These methods will be described in the following sections.

1.2.1 Non contact type data acquisition techniques

Laser scanning CMM has a non contact probing system. A beam from the laser scanner is swept across the surface of the component to record the points. Figure 1.4 shows the basic schematic of a laser scanner. The laser beam spreads out in a plane that forms the line of light on the part under measurement. The sensor mounted in the probe takes the range measurement over the entire line of laser beam on the part under measurement at the same time. The advantage of laser scanning based CMM is that they have high scanning rate and they can also be used for thin objects. They also provide measurement points from different view angles [3]. The disadvantage with laser CMM is that the data points collected are very noisy in nature and it requires denoising of the data points before using them for tolerance evaluation.
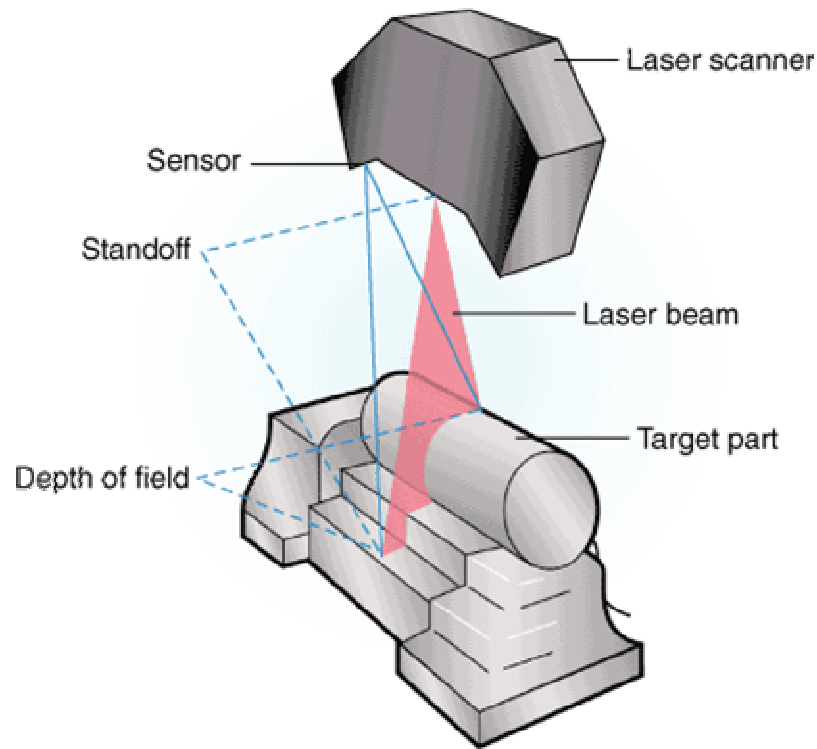
Figure 1.4: Laser scanning coordinates measuring machine [30]

1.2.2 Contact type data acquisition techniques

Touch trigger probe based CMM are the most widely used data acquisition systems in industry. The probe consists of a stylus and a stylus tip which is spherical in nature. As shown in Figure 1.5 the probe is held in a single unique position by means of six contacts of three cylindrical rods with six balls and a light spring preload to maintain this position when no external force is applied. The six contacts are electrically wired in series and have a very small resistance. Therefore, when the probe touches the surface, and deflects the stylus tip against the preloaded spring, the resistance of one or more contacts increases and when the generated voltage becomes more than a cutoff, the circuit trips and the x, y, z position of that point freezes. It is to be noted that it is the center of the stylus tip that is recorded in the measurement [29].

Thereby, the probe radius needs to be compensated for, in approach direction, in order to calculate the measurement point on the surface.
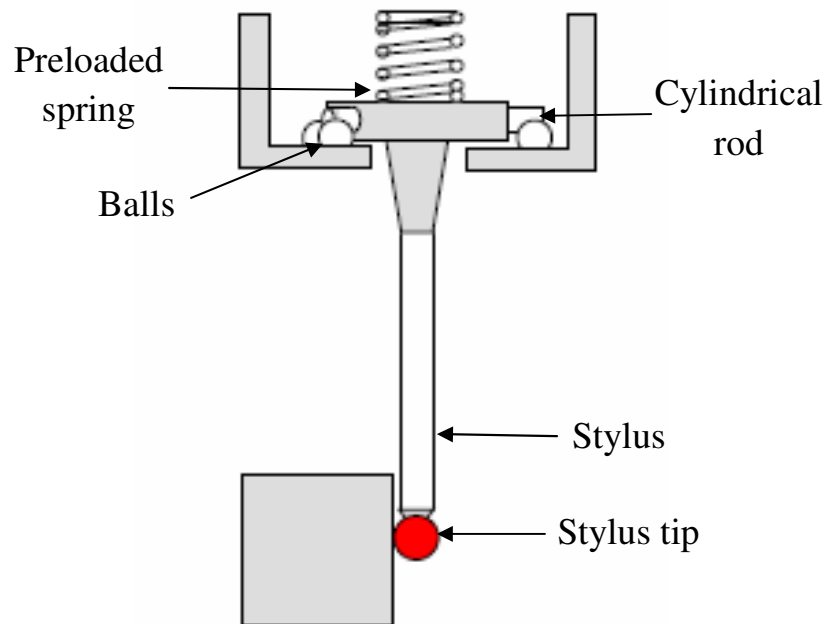
Figure 1.5: Touch trigger based probe system of a coordinate measuring machine [29]

1.2.3 Measurement data characteristics

The measurement data points thus acquired through CMM are further considered for the evaluation of tolerances to determine the conformance or non-conformance of the manufactured part with the design model. However, the measurement points cannot be directly used for tolerance evaluation purpose. There are two inherent problems associated with the measurement data: Discrete nature and measurement uncertainty.

ASME standard defines tolerance definitions by considering all the points of the surface under inspection [13]. However, the measurement points obtained from the inspection process are discrete in nature therefore they represent only a small sample of the whole surface. Hence,

there is always some information missing between the one provided and the one needed for evaluation.

The second issue with the measurement data is measurement uncertainty. All the measurement processes are inherently imperfect in nature and therefore the measured points do not represent the actual values of measurement. This dispersion of actual value about the measurement value is known as measurement uncertainty. The measurement uncertainty is quantified by standard deviation. It represents dispersion about the measurement point within which the actual value of measurement may lie. Probe pre travel, probe bending, probe size imperfection, manufacturing component form error are some of the contributing factors towards measurement uncertainty [10]. Due to these inherent problems with the measurement data points, one must be careful that the measured points represent the actual surface sufficiently; otherwise erroneous conclusions may be drawn during tolerance evaluations [18].

1.3   Impeller blade inspection

The work in this thesis focuses on the tolerance evaluation of impeller blades. Impellers are the rotating devices which convert the electrical energy of motor into the kinetic energy of air. As shown in Figure 1.6 impeller has a complicated freeform profile. Impeller has several blades attached to the hub along the hub axis. The blade surface is defined by the pressure surface, suction surface, leading edge and trailing edge. Other main components of the impeller are also shown in the figure. Generally, hub and blades are manufactured as a single component by using five axis CNC machine tools.

The complex geometry of impeller blades poses significant challenges to data acquisition and as well as to the parameter and geometric tolerance evaluation [6]. The first difficulty is in setting up the part coordinate system which requires information of 6 points on the manufactured

impeller blade. Some of these points are defined on the curved surfaces and are actually difficult to measure due to the lack of surface normal information which is required for the approach direction [6]. Furthermore, impeller blade has sharp geometry at the ends (leading edge and trailing edge), thereby making it difficult to measure the points in those narrow sections [7].
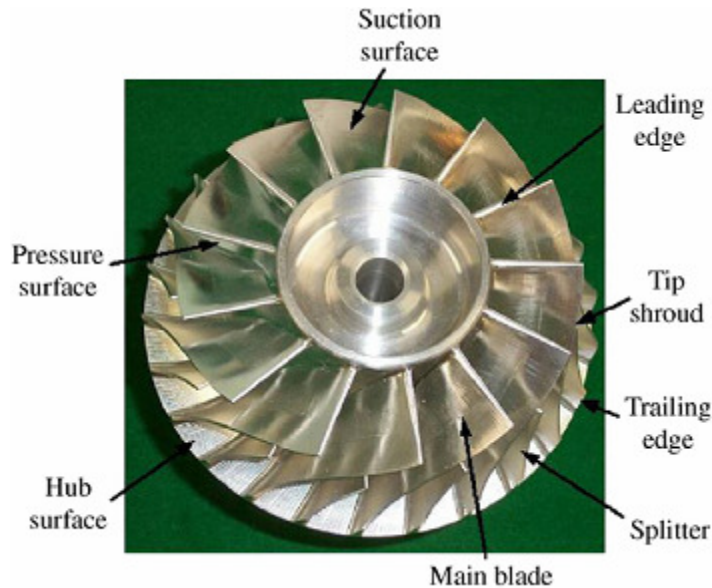
Figure 1.6: Typical configuration of a machined impeller [3]

Using probe type coordinate measuring machines, impeller blades are inspected along the pre-specified sections as shown in Figure 1.7. The surface normals and the target data points for measurement are generated from the CAD model of the impeller blade. The recorded center data points of stylus tip are further compensation for probe radius to achieve the points on the actual surface. Due to more stringent tolerance requirement on the leading and the trailing edge, the measurement data points are densely measured on theses edge in comparison to the measurement points on the pressure and suction sides. The complete impeller blade inspection requires the evaluation of geometric parameters and tolerance for the pre-specified airfoil sections. There are two popular methods of the impeller blade measurement data analysis. The first trend compares the measurement points along the cross sections for complete pressure and suction surfaces with the CAD surface [7], thereby making it a 3D inspection. The second strategy involves the

8

comparison of individual sectional measurement data with the corresponding CAD section [6]. As the cross sections are on constant height, therefore, only x, y coordinates of the measurement data are considered for the evaluation and the inspection analysis becomes 2D. This thesis adopts the second strategy of sectional data analysis as the tolerances are specified for the individual two dimensional cross sections; therefore the evaluation will be consistent with the specification. Any deviation in the z coordinate of measurement points is assumed to be considered in the measurement uncertainty. The next section details out the geometry and associated tolerance with the impeller blade cross section.
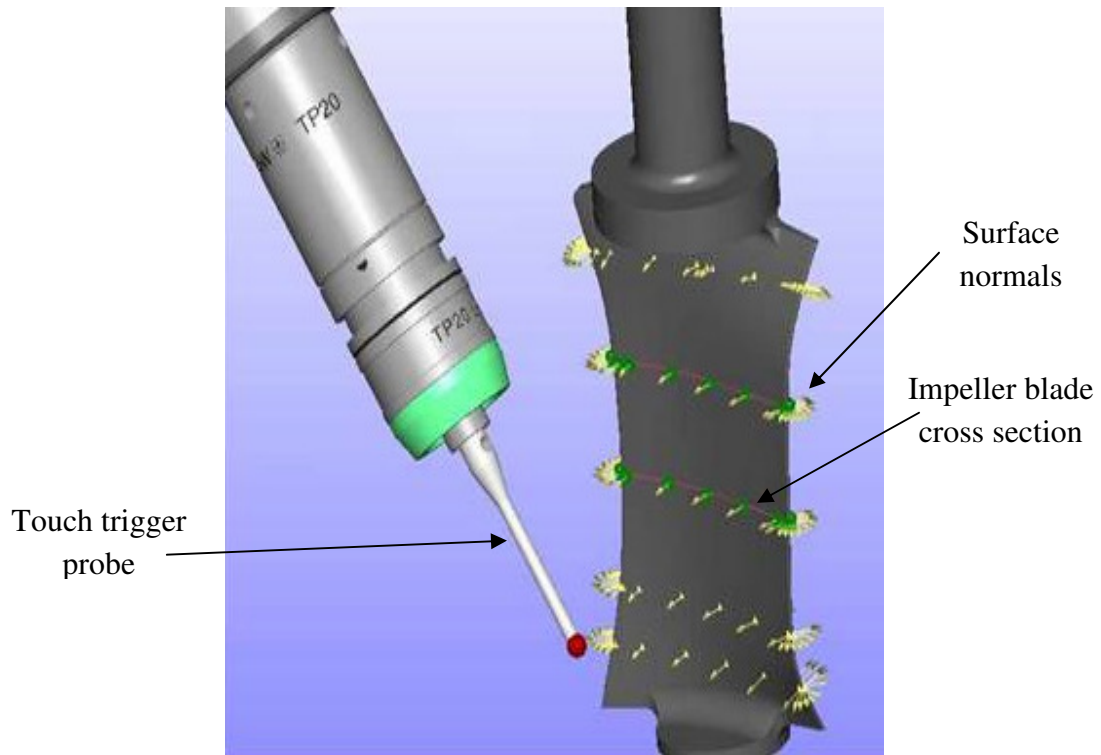
Figure 1.7: Impeller blade inspection along pre-specified airfoil sections using a touch trigger probe [28]

1.4 Airfoil section geometry and tolerances

The airfoil section is the cross section of the impeller blades along which the measurement data points acquired. As this dissertation focuses on the sectional tolerance

9

evaluation, therefore a brief background on the geometry of airfoil section and associated tolerance is needed.

1.4.1 Geometry

The basic design unit of an impeller blade is a two dimensional airfoil section. Impeller blade surface is constructed by stacking these airfoil sections on top of each other along a stacking axis. A typical airfoil is shown in Figure 1.8.
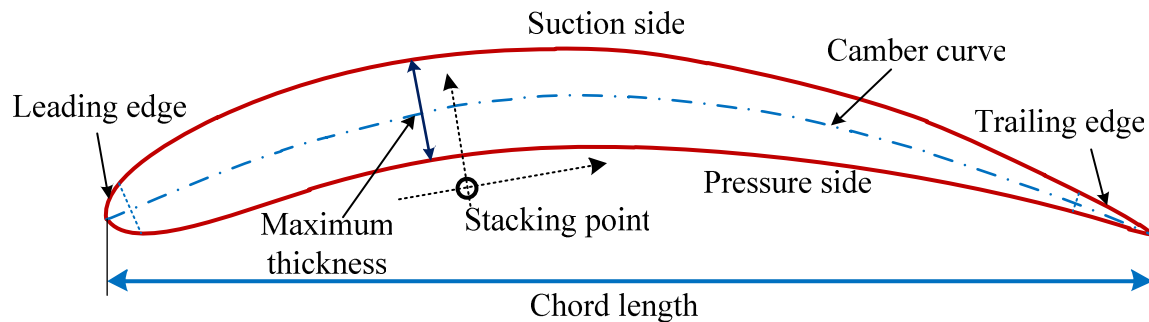
Figure 1.8: Typical airfoil section

Leading edge is the nose point of the impeller blade and this is the first point where the air strikes the blade. The air gets separated from the leading edge to pressure and suction sides. As this edge is responsible for air separation, it is imposed with more stringent tolerances in comparison to rest of the section. Trailing edge point is the end point of the impeller blade from where the air leaves. Leading and trailing edge are generally designed in circular or elliptical shape. The suction side and the pressure sides are responsible for creating a passage through which the air passes. Suction side is the curve on the convex side of the blade where the air pressure is decreased. Pressure side is the curve on the concave sides where the air pressure is increased. These sides have less curvature variations unlike the leading and trailing edges. Camber curve is the mid curve of airfoil section and is also known as spine curve. Any point on

the camber curve is equidistant from the pressure and suction sides. Chord length determines the width of the impeller blade. Stacking point is the center of gravity of the airfoil section. For designing the impeller blade, the airfoil sections are placed along an axis with their stacking points lying on the axis.

1.4.2 Tolerances

The geometric parameter and tolerance requirements for pressure, suction side and leading, trailing edges are different due to different functional requirements. Therefore, tolerance analysis of airfoil section is performed separately for leading, trialing edges and pressure, suction sides. The scope of this thesis is limited to the tolerances associated with the pressure and suction sides.

(i) Profile tolerance: Profile tolerance controls the form of the pressure and suction surfaces. As shown in Figure 1.9 profile tolerance is assigned as a zone about the design curves of the pressure and suction sides, within which the manufactured profile is allowed to vary. To evaluate the profile error of a manufactured feature, a minimum zone formed by the measurement points about the design feature is evaluated. If the evaluated zone lies within the specified tolerance zone, then manufactured feature meets the quality requirements. As per ASME standard [13], profile tolerance can be of three different types: Bilateral symmetric, bilateral asymmetric, and unilateral. This classification is done based on the permissible deviation on each side of nominal feature. (Profile tolerance is extensively described in Chapter 3.)
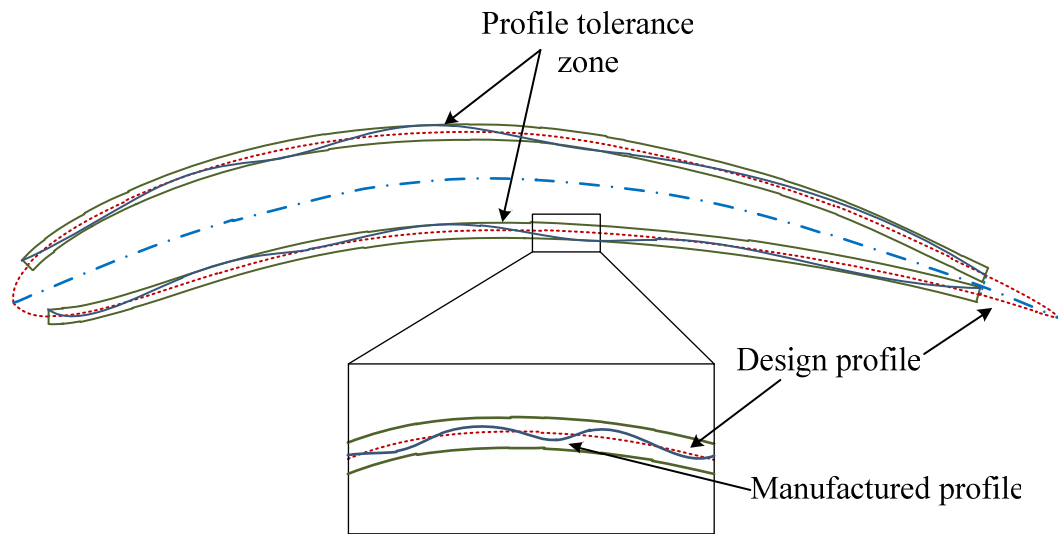
Figure 1.9: Profile tolerance zone on pressure and suction side of an airfoil section

(ii) Thickness dimensions: Thickness dimensions control the distance between the pressure and suction sides at key locations as shown in Figure 1.10. These parameters strongly affect the aerodynamic characteristics of an airfoil. Thickness dimension is defined as the distance between the pressure and suction side when measured perpendicular to the camber curve. Maximum thickness, leading edge thickness, and trailing edge thickness are common thickness dimensions for evaluation.
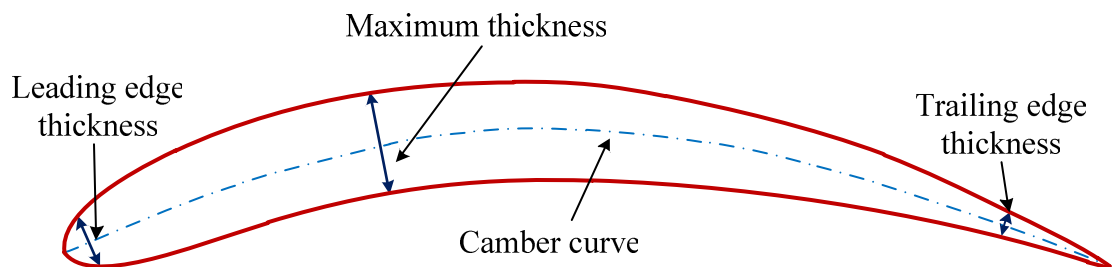
Figure 1.10: Thickness dimensions of an airfoil section

(iii) Thickness control zone: Thickness control zone controls the overall variation of the pressure and suction sides of an airfoil section. As airfoil section has a continuously varying shape, profile tolerance and thickness dimensions are alone not sufficient to control the overall variation. Profile tolerance only controls the form of individual surfaces and thickness

12

dimensions only controls the thickness at a localized points. The thickness control zone does not govern the leading and trailing edges. Thickness control zone tolerance becomes more important in the case of blades with large chord length where pressure and suction sides are long enough to be controlled by the thickness dimensions.
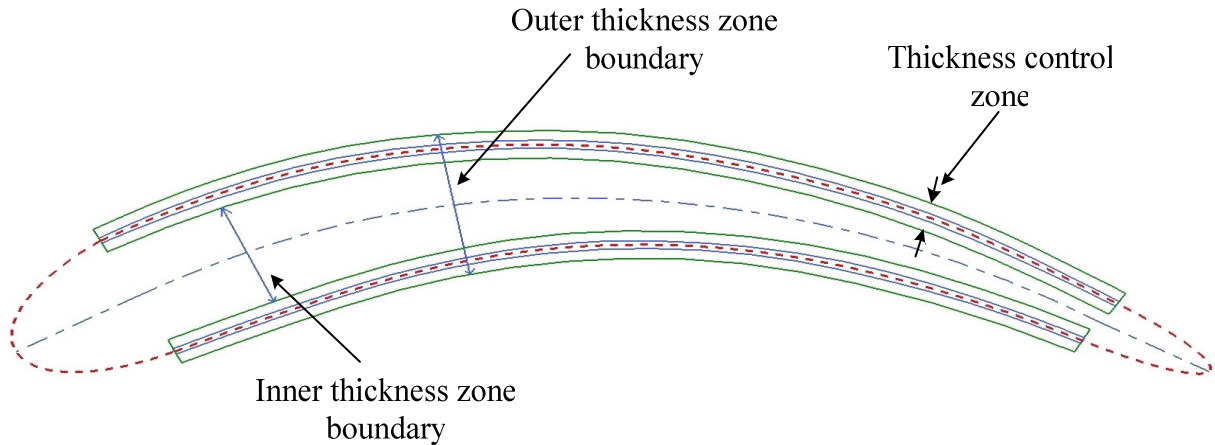
Figure 1.11: Thickness control zone on the pressure and suction sides of an airfoil section

Thickness control zone is a relatively less known tolerance measure for airfoil sections. However, it can be derived analogous to the size tolerance applicable to the prismatic components. As size tolerance defines an allowable tolerance zone for a component by creating a maximum permissible deviation boundary and minimum permissible deviation boundary [13]. Similarly, as depicted in Figure 1.11 thickness control zone is also defined by an inner boundary and outer boundary within which the manufactured profile of pressure and suction sides are allowed to vary.

1.5   Existing research work

The existing research work in the domain of airfoil blade inspection is particularly focused on the blade section measurement and development of the methods for evaluation of blade parameter and geometric tolerances. Due to the high curvature of airfoil section at the

leading edge and trailing edge, significant variation may exist in the manufactured section and the measurement paths designed based on the CAD model. Therefore, existing research papers for airfoil section mainly focus on the path planning for blade section measurement. Furthermore, the analysis of measurement data for blade inspection is also an important and challenging task. As the design documents only define parameters and tolerances that need to be evaluated, it does not tell us how these values are computed. Hence, methods need to be devised to evaluate the specified tolerance and parameters associated with airfoil sections [6].

Pahk et al [7], proposed a measurement technique for parts having very thin and sharp curve features, which is the case with airfoil blades. They developed two stage path planning technique for data measurement. The acquired measurement data points were further analyzed for profile tolerance evaluation of pressure and suction surfaces and radial tolerance of leading and trailing edges. The objective function for profile tolerance evaluation was formulated as the minimization of maximum error between the measurement points and the corresponding closest points on the CAD surface. Subdivision algorithm was used to determine the closest points on the CAD surface corresponding to the measurement points. The complete blade surface was analyzed for profile tolerance at once. However, in practice the profile tolerance requirement for pressure and suction sides are different than for the leading and trailing edges. Therefore, combined analysis may lead to a higher error on leading and trailing edges.

Hsu et al. [6] proposed a method for blade measurement based on the back off direction. The back off direction ensured that the probe radius is compensated accurately to achieve the points on the actual surface and to improve the accuracy of measurement. Blade measurement was performed along sections in such a way that the acquired measurement data were in equal height for a specified section which enabled the 2D inspection of individual sections. The measurement data set was initially aligned based on the leading and trailing edge point. Profile

14

tolerance for leading edge, pressure side and suction side of a sectional curve were analyzed individually. The profile tolerance problem was formulated as the root mean square error between the data points and CAD points. Thickness dimensions, blade displacement, chord length and twist angle were other parameters which were also evaluated. This work suggested a localized error evaluation for each feature on section.

Chen et al. [8] completely focused on the area of blade parameter evaluation. Similar to Hsu et al., they also performed blade parameter evaluation for individual airfoil sections. Their main focus was on the evaluation of the chord length, leading and trailing edge radii and twist angle analysis of impeller blade.

In a parallel domain of marine propeller inspection, Allen et al. [25] developed a software PROPAR for analyzing the propeller blade parameters from the CMM inspection data. They emphasized on the localized tolerance determination for leading and trailing edge and pressure and suction sides. Their argument was that localized analysis will give more accurate description of machined surface variation. They best fitted the measurement data on the design feature using a least square objective function.

Patrikalakis et al. [9] fitted the NURBS surfaces in the measurement data of a marine propeller. To evaluate the tolerance zone, least square fitting was employed. They further reconstructed the camber curve of a single hydrofoil section and predicted the thickness dimension variation in manufactured hydrofoil section.

Peiqing et al. [26] performed NURBS based fitting on the measurement data points of a turbo blade. The reconstructed surface was interpolated through the measurement data points and then different parameters were evaluated based on the reconstructed model. As, the measurement data always carry certain measurement uncertainty, therefore an interpolation based method may

not approximate the surface close enough to actual surface, and this may lead to the wrong parameter calculation.

1.6   Research scope

In all the papers cited above, the profile tolerance has been evaluated assuming it to be a bilateral symmetric tolerance. Asymmetric and unilateral type profile tolerance analysis is not even considered for airfoil sections. Industrial practices suggest that pressure and suction sides of airfoil sections can also be assigned with the unilateral or bilateral asymmetric types of tolerances. Therefore, profile tolerance analysis for airfoil section should also focus on evaluating unilateral and bilateral asymmetric tolerances. In general domain of profile tolerance evaluation, literature review suggests that methods of least square fitting and minimax fitting are widely used methods. The least square fitting minimizes the sum of squares of deviations. However, it tends to overestimate the maximum error, which may result in non-conformance with the specified tolerance [23]. Furthermore, least square fitting always produces a zone about the design geometry. Hence, it will never be able to confirm with unilateral type profile tolerance. On the other hand, the minimax fitting always produces a symmetric zone which is only consistent with the bilateral symmetric type (Chapter 3 in detail discusses the present literature in profile tolerance evaluation domain). Therefore, it is evident that a method is still lacking which can evaluate all possible types of profile tolerances.

Furthermore, the above cited papers only consider profile tolerances and thickness dimensions parameter for inspecting the pressure and suction sides of an airfoil section. These two parameters are not sufficient to control the overall variation in airfoil shape. The pressure and suction sides create the throat gap between two consecutive blades and thus control the air

pressure and in turn the performance of the impeller. Hence, thickness control zone which controls the variation between the pressure and suction sides should also be evaluated.

The listed literatures considered the measurement data points directly for the parameter and geometric tolerance evaluation. The measurement uncertainty was not considered at all in the documented studies. Because of the measurement uncertainty, even after the optimal positioning, the measurement data do not exactly represent the actual points on the inspected object surface. Therefore, any tolerance analysis based only on the measurement points can mislead the conclusions. Hence, it is imperative to consider the measurement uncertainty during tolerance evaluation.

1.7 Research objective

Based on the research scope described in pervious section, the overall research objective is mainly divided into two tasks. The first objective is to develop a unified methodology for profile tolerance which can address evaluation of all types of profile tolerances: bilateral symmetric, bilateral asymmetric, and unilateral. For given sectional measurement data points, the method is expected to predict the conformance of evaluated minimum zone with the specified tolerance zone. The second objective is to develop a method for evaluation of thickness control zone from the measurement data points of pressure and suction sides. Furthermore, the thesis also tries to consider the concept of measurement uncertainty for error evaluations. For simplicity of implementation and input for case studies some assumptions have been considered, which are as follows:

1. The measurement uncertainty value is assumed to be given for all the calculations.
2. The measurement data points of airfoil section are assumed to be segmented for pressure and suction sides.

3. The nominal geometry of pressure and suction sides is assumed to be simple Hermite cubic curves.

4. It is assumed that the probe center data for measurement is already compensated for the probe radius and resulting points are being considered here for the evaluation of tolerances.

The subsequent chapters in this thesis address each of the objectives. Chapter 2 discusses the accommodation of measurement uncertainty by reconstruction of profiles for pressure and suction sides from the measurement data. Chapter 3 focuses on the evaluation of unified method for profile tolerance evaluation. Chapter 4 is dedicated to the thickness control zone evaluation. The case studies are presented at the end of each chapter to discuss the observations and results. Chapter 5 summarizes the contributions of this research, its limitations and possible future work.

2 Profile Reconstruction

2.1   Introduction

To evaluate the tolerances associated with any component, measurement points need to be compared with their respective design features. However, because of the measurement uncertainty, the acquired measurement points do not represent the actual points on the inspected object surface. Therefore, tolerance evaluation based directly on the measurement points might lead to wrong conclusions. Furthermore, the evaluation of thickness dimension parameters of an airfoil section requires profile reconstruction of camber curve, pressure side and suction side curves. Hence, it is imperative that the profile is reconstructed from the measurement points. However, the actual profile can never be exactly generated from the measurement data, it can only be approximated within a given measurement uncertainty. The points generated from the reconstructed profile are then compared against the design profiles for evaluating the specified tolerances.

A methodology has been proposed in this chapter to reconstruct the pressure and suction profiles that approximates the actual profile within a given measurement uncertainty. Thereafter, camber curve is derived from the constructed profiles of the pressure and the suction sides. The chapter outlines the concept of measurement uncertainty for CMM, followed by methodology for profile reconstruction of the pressure and suction sides, and the camber curve. Subsequently, case studies with discussion are also presented.

2.2   Measurement uncertainty

The term uncertainty expresses the doubt on the validity of measurement values. Measurement uncertainty is a parameter associated with the measurement results, which defines

the dispersion about measurement values within which the actual value of measurement can reasonably lie. Due to measurement uncertainty, a reliable assessment on conformance and non conformance of the manufactured surface to the design specifications cannot be made. In coordinate measurement, there are multiple factors which affect the measurement results and they are being described in the following section.

2.2.1 Factors contributing to measurement uncertainty

The measurement uncertainty for CMM results is caused by many factors as shown in the Figure 2.1 . These factors can be broadly classified into environment, operator, work piece, measurement strategy, and measuring instrument.
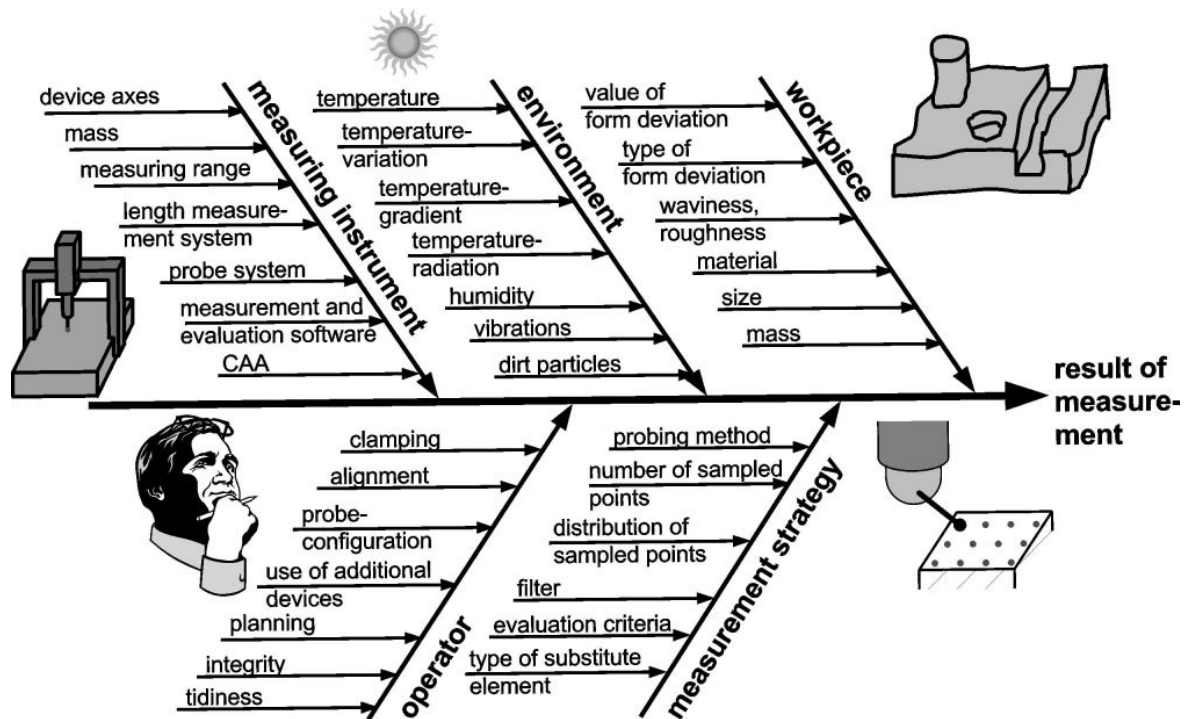
Figure 2.1: Factors affecting coordinate measurement results [10]

Influence of environment broadly includes variations in temperature, vibrations and dirt particles. A change in temperature from the reference temperature causes dimension changes in CMM and work piece [10]. To minimize the vibration, damping devices are used. And to minimize the dirt particles filters are used. Operator also influences the outcome of measurement

during alignment and clamping of the component, selection of probe and assigning probing force. The surface roughness, waviness, form and other geometric factors of work piece also contributes to the measurement uncertainty.

The key contributors to the coordinate measurement uncertainty are the probing method and probe system itself. CMM probe operation is influenced by probing angle, probe orientation, stylus configuration, stylus materials and work piece condition. Figure 2.2 illustrates a situation where the actual target point is missed during measurement by CMM. The presented situation may arise because of the multiple factors such as work piece condition, inaccurate approach direction calculation etc. As the figure shows, to measure a point on the object surface, the stylus probe is moved in an approach direction and as soon as the surface of stylus tip touches the object surface, the coordinates of the center of the stylus tip are recorded as the measurement point. However, even after compensating for the probe radius in approach direction, the obtained compensated point is not the actual targeted point on the surface. All the factors influencing the measurement are considered to calculate a measurement uncertainty which gets associated with the measurement results.
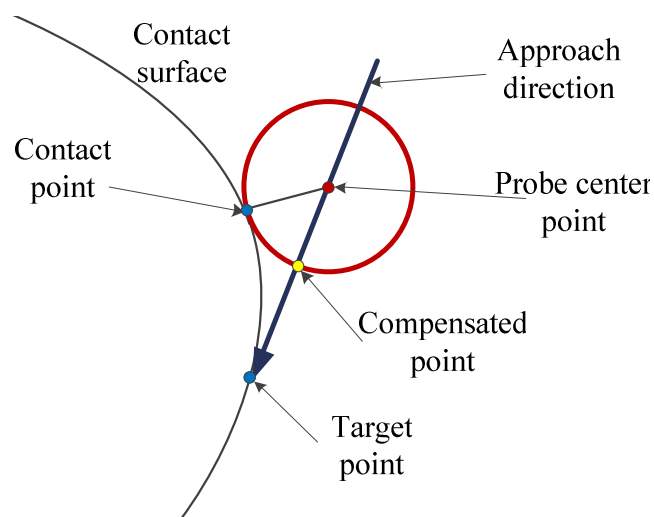
Figure 2.2: A typical case of a missed target point during measurement using touch trigger probe

21

2.2.2   Measurement uncertainty calculation

The measurement uncertainty is a statistically derived term and generally characterized by a standard deviation of a normal Gaussian distribution as shown in Figure 2.3. For calculating the combined measurement uncertainty budget u_c, individual uncertainty contributions from the individual factors are calculated and lumped together based on the guidelines provided by Guide of measurement uncertainty [5]. For practical applications, measurement uncertainty is expressed as an expanded measurement uncertainty which is defined as an interval about the measurement result such that interval is expected to enclose a large fraction of the distribution of actual values that can be attributed to the measurement value y. A coverage factor k is multiplied to u_c for getting the expanded uncertainty $U = ku_c$.The result of a measurement is then expressed as $y \pm U$, which means that the true value which can be attributed to measurement value y will lie in interval of $y - U$ to $y + U$ [5]. The coverage factor corresponds to a desired level of confidence. The value of k has been set as three in this work, which defines an interval of $\pm 3u_c$ and corresponds to a confidence level of more than 99%. The calculation of expanded measurement uncertainty U is not considered under the scope of this work and is assumed to be given for all the calculations in this work.
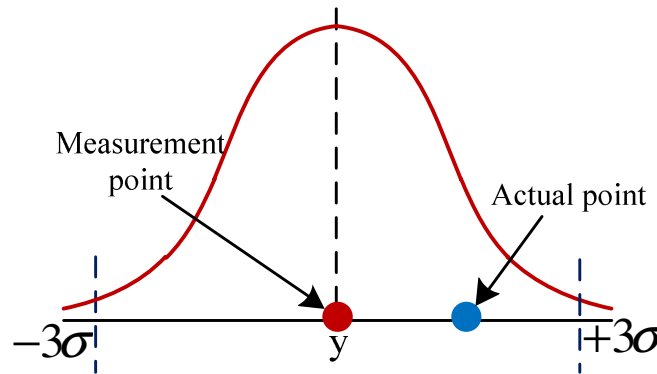
Figure 2.3: Concept of measurement uncertainty

22

2.3 Methodology for profile reconstruction

This section presents the methodology behind the profile reconstruction of pressure and suction sides from the measurement data points. It needs to be reiterated here that it is impossible to reconstruct the actual profile from the measurement data points. This work attempts to utilize the measurement uncertainty information attached to measurement results for the reconstruction of the pressure and the suction sides. The methodology for profile reconstruction uses two concepts: Feasibility condition and minimum undulations, which are explained as follows.

2.3.1 Feasibility condition

This expanded measurement uncertainty interval can be regarded as a circle with diameter U centered on the measurement data points as shown in Figure 2.4. For each measurement point, the corresponding actual point will lie, with high probability (more than 99%), inside the measurement uncertainty circle. Hence, a curve passing through all the uncertainty circles can be considered as a feasible approximation of the actual curve as it meets the measurement uncertainty definition. This property of a curve which passes through all the circles is termed as 'feasibility condition' in this work. As depicted in the Figure 2.5 there are numerous curves which can pass through all the circles and satisfy the feasibility condition. Therefore an addition criterion is required to pick the profile curve.
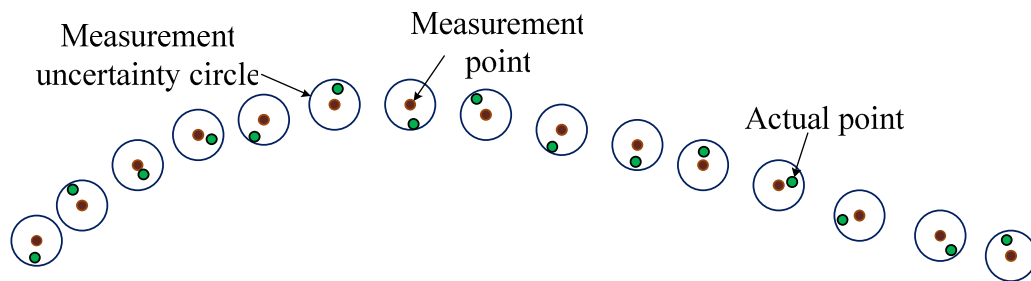
Figure 2.4: Measurement uncertainty circles about the measurement points. Actual points lie inside these circles.
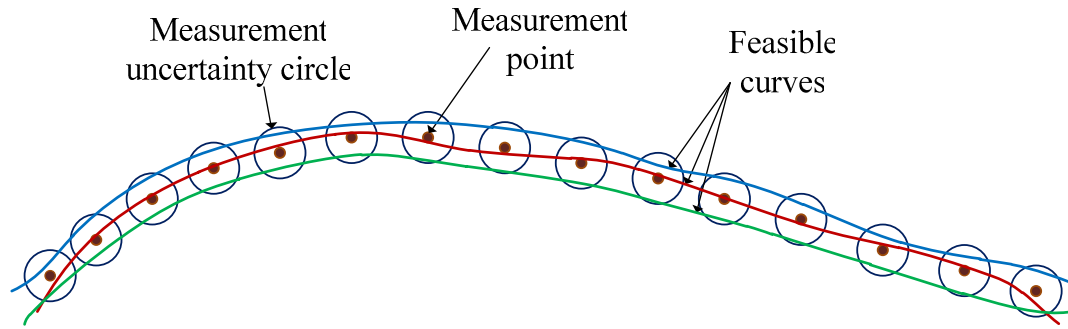
Figure 2.5: Definition of a feasible curve: a curve which passes through all the measurement uncertainty circles

2.3.2 Minimum undulations

The second property is derived from the geometry of the pressure and suction sides. The geometry of pressure and suction sides suggests that the profile curves are smooth in nature and are without any undulations. Hence, a feasible curve with minimum undulations is selected as a closer approximation to the actual curve. For profile reconstruction, the concepts of feasibility condition and minimum undulations are used in conjunction. However it is to be noted that meeting feasibility condition is a primary criterion. To elaborate further on this, the curve shown in Figure 2.6 shows zero undulations. However, despite satisfying this condition, the curve fails to approximate an actual curve since it is not able to satisfy the feasibility condition. Figure 2.7 suggests an alternate curve fitted with two curves. The fitting has increased undulations however, it satisfies the feasibility condition hence, this deemed to be a closer approximation with actual curve.
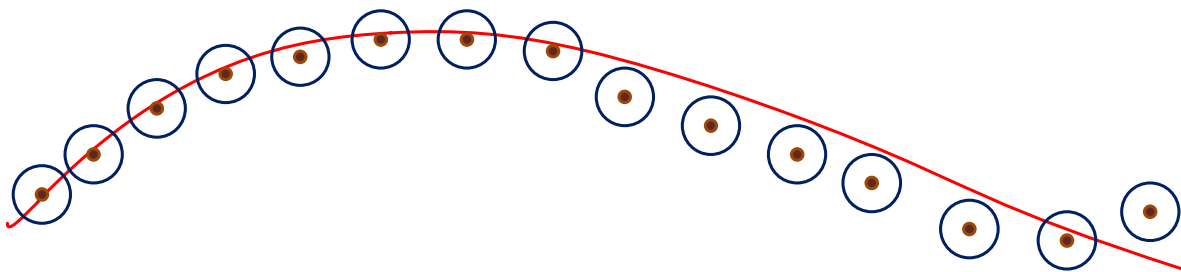
Figure 2.6: Curve with zero undulation but violating the feasibility condition

24
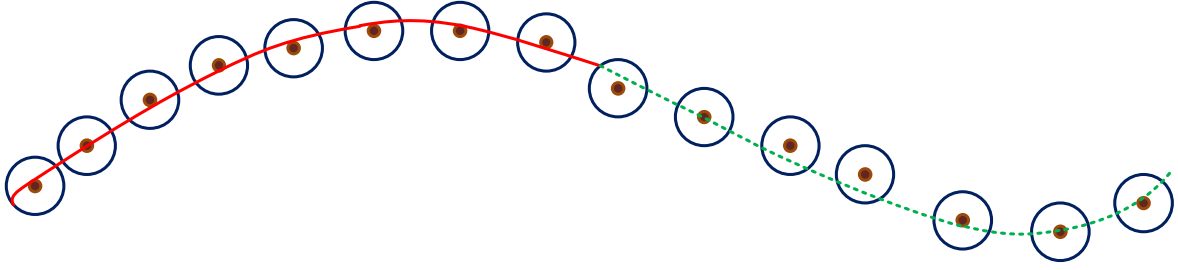
Figure 2.7: Alternate curve fitting with an undulation and meeting the feasibility condition

2.4 Mathematical formulation

As the measured points carry uncertainty and are not exact points on the actual profile, the approximation-based method for curve fitting is adopted over the interpolation-based method. Least-squares best fitting is used in this work, as it would give the best approximate of the actual profile curve if the mathematical expression of the fitted curve is formulated correctly. More importantly, the measurement uncertainty, which is assumed to be normally distributed, is readily considered in the least-squares fitting. The objective function for the best fitting is formulated as sum of squares of residuals of each data point from the fitted curve and can be represented by Equation (2.1).

$$Obj = \sum_{i=1}^{n} e_i^2 \tag{2.1}$$

where e_i is the fitted residual and is calculated as the perpendicular distance between the ith data point and the fitted curve and n is the number of data points. The concept of feasible curves and the criterion of minimum undulation introduced in the previous subsection 2.3.1 and 2.3.2 are explicitly considered in the curve fitting algorithm and are presented below.

(i) Feasible Curves: This is the primary consideration in reconstructing the pressure and suction profile curves. If the reconstructed curve meets the feasibility condition, it is considered a feasible solution. A comparable quantity with the expanded measurement uncertainty is to be

25

derived from the fitted residuals. More specifically, the standard deviation σ_r estimated from the fitted residuals is multiplied by six and compared against U. This ensures that the majority of the fitted residuals would lie within the measurement uncertainty circles. The fitted curve can then be deemed as being constructed within the measurement uncertainty U. The mathematical expression for this condition is as follows,

$$6\sigma_r \leq U \tag{2.2}$$

with
$$\sigma_r = \sqrt{Obj \big/ (n-1)}$$

(ii) Minimum Undulation: Many fitted curves would meet the feasibility condition of equation (2.2). The fitted curve with the minimum undulation is desired in this work and is attained via a progressive curve fitting scheme. For the fitting purpose, a cubic degree curve is chosen as it is more flexible in comparison with the second degree curve and would be better for fitting the data points of suction or pressure sides. Higher degree curves are more flexible, but in order to meet the feasibility condition, they can produce a curve with several undulations. Therefore, to keep the undulations to a minimum, a progressive fitting approach is adopted. In this approach, first a single cubic curve segment is fitted in the measurement data points, and then fitting is check against the feasibility condition. If the condition is not met, an additional curve segment is added to the fitting and the resulting composite curve is checked once again against the feasibility condition. The number of employed curve segments increases until the feasibility condition is satisfied.

For progressive curve fitting, piecewise C^1 continuous parametric Hermite cubic spline curves are employed. Figure 2.8 shows a typical Hermite curve. The curve is characterized by end point vectors and end point tangents. For piecewise fitting, the Hermite form of curve is more intuitive as at the junction of two curves, the joint point vector and the joint point tangent

vector will be common to both the curves. The joining point of two consecutive curves is also known as knot point.
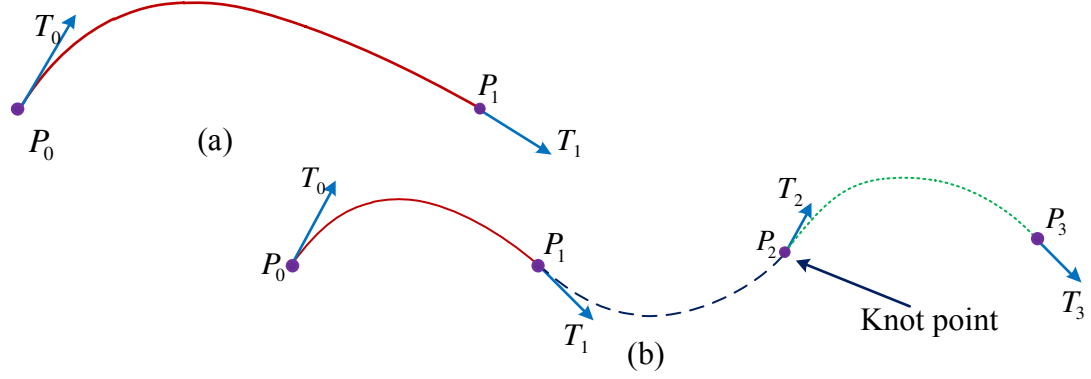
Figure 2.8: Hermite curves (a) Single Hermite curve (b) Piecewise Hermite curves

The parametric equation of a cubic Hermite curve is mathematically represented as follows:

$$H = \underbrace{\begin{bmatrix} t^3 & t^2 & t & 1 \end{bmatrix} \begin{bmatrix} 2 & -2 & 1 & 1 \\ -3 & 3 & -2 & -1 \\ 0 & 0 & 1 & 0 \\ 1 & 0 & 0 & 0 \end{bmatrix}}_{[B]} \underbrace{\begin{bmatrix} P_0 \\ P_1 \\ T_0 \\ T_1 \end{bmatrix}}_{[C]} \tag{2.3}$$

where **H** represents the Hermite curve equation. The formulation consists of a basis function matrix **B**, which is dependent on the parameter value t for each point and the curve coefficient matrix **C**.

2.5 Progressive piecewise curve fitting

There are a number of research works available in the domain of piecewise curve fitting. The method implemented in this thesis work is adopted from them and particularly based on the work by Cox [11]. To fit the piecewise curves, fixed knot fitting method is adopted. To minimize the objective function given in Equation (2.1), an alternating method suggested by Hoshek and Rogek [12] has been used in this thesis. The alternating method breaks down the original

problem into two smaller problems that can be implemented easily. As a first step, the method suggests a suitable estimation of parameter values of t corresponding to each data point. Thereafter, once the parameter value is known, the objective function formulation is reduced to a linear least square problem and curve coefficients can be solved using a closed form solution. As the initial parameterization is arbitrary in nature, hence, for better estimation, re-parameterization is performed based on the fitted curve. Figure 2.9 shows the flowchart for over all profile reconstruction method. The method iterates between curve coefficient determination and re-parameterization till the objective function value is minimized. The subsequent sections discuss the important steps by presenting formulations for single curve fitting. The discussion also suggests respective modifications in each step for a piecewise curve fitting.
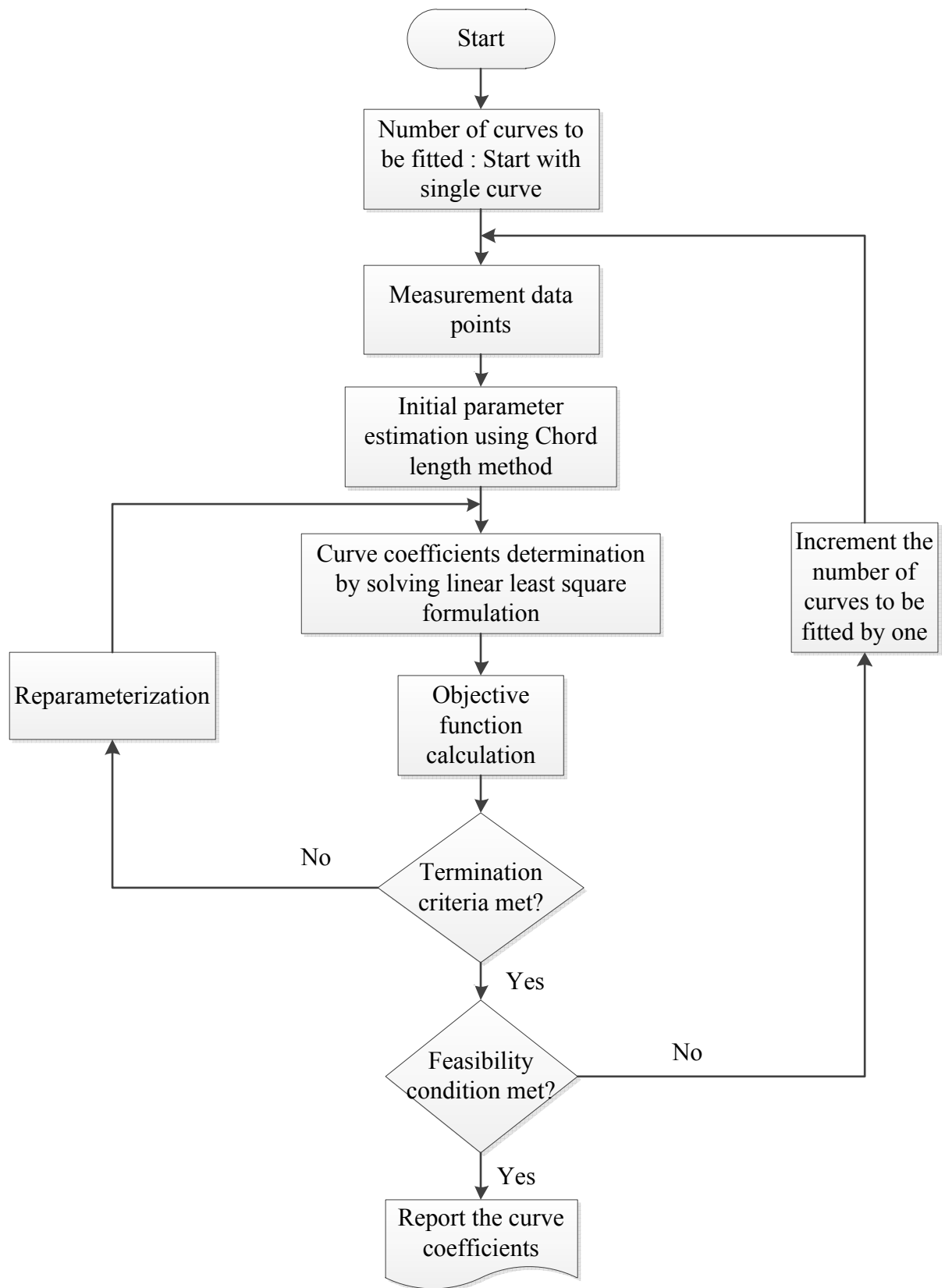
Figure 2.9 Flowchart for progressive curve fitting to reconstruct the profiles of pressure and suction sides from the measurement data points

2.5.1 Chord length parameterization

To initialize the iterative curve fitting, an initial set of parameters needs to be estimated to calculate the curve coefficients. For this, an already established method of chord length parameterization is used [31]. Chord length parameterization is based on the principle that, the length of a curve between two consecutive points will be very close to the Euclidean distance between the two points. The distance between two consecutive points is being referred to as chord length. And by extending this argument, length of the curve will be very close to the sum of the chord lengths of data polygon. Hence, if the initial parameter values are assigned in the ratio of distribution of chord length over the data polygon length, then this will provide a good initial condition for the parameter estimation.
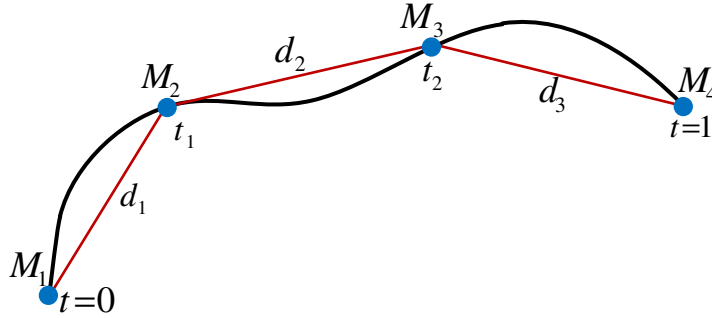
Figure 2.10: Chord length parameterization from measurement data points

Let the CMM points be denoted by M_i as shown in Figure 2.10. where $i = 1....n$ and the distance between two consecutive points be denoted by d_i, where $i = 1....(n-1)$. d_i is an Euclidean distance between point M_{i+1} and M_i. The length of the data polygon can be calculated from Equation (2.3):

$$L = \sum_{i=1}^{n-1} d_i \tag{2.3}$$

r_k is defined as the ratio of sum of chord lengths over the length of data polygon,

$$r_k = \frac{\sum_{i=1}^{k} d_k}{L} \tag{2.4}$$

The parameter value t of a single curve varies from 0 to 1, and the parameter value can be assigned as following:

$$\begin{aligned} t_0 &= 0 \\ t_k &= r_i \\ t_1 &= 1 \end{aligned} \tag{2.5}$$

If a single curve fitting is not able to satisfy the feasibility condition, the number of curve segments are increased and fitted to the measurement data points. In this situation, for determining the initial set of parameter t, the data points are uniformly divided in as many numbers of sets as curve segments. In case of uneven distribution, the remaining points are assigned to the last curve segment. For each individual data set, individual data polygon is calculated and parameter t is estimated using chord length method. In case of multiple curve segments, the range of parameter t differs for data polygons and varies from 0 to 1for the first curve segment, 1 to 2 for the second curve segment and so on.

2.5.2 Curve coefficient determination

Once the parameter values t corresponding to each parameter are known, the objective function formulation reduces to a linear least square problem as follows,

$$[B][C] = [M] \tag{2.6}$$

Here, matrix **B** is a basis function matrix for all data points and can be calculated from the estimated parameter value t. **M** represents the matrix consisting of x, y coordinates of all data

points. $\mathbf{C}$ is the unknown curve coefficient matrix. The solution of Equation (2.6) is available in closed form and curve coefficients can be calculated by using following equation,

$$[C] = ([B^T][B])^{-1}[B^T][M] \tag{2.7}$$

Using the evaluated coefficients, the curve is constructed and normal residuals e_i for all the data points are calculated to determine the objective function value. For piecewise curve fitting, the basic formulation for solving the curve coefficients remains same. The size of unknown matrix $\mathbf{C}$ changes and it depends on the number of curve segments employed for fitting. For example, for two curve segments, there will be 6 unknowns as the point vector and tangent vector for knot point will be common to both the curves.

2.5.3 Re-parameterization

The initially fitted curve is based on the approximated values of parameters and therefore, the parameter value needs to be re-estimated. Re-parameterization is performed based on the 'closest point' concept. For each CMM data point, a closest point on the fitted curve is determined using the nearest neighbor algorithm. The parameter values of these closest points are recorded and linearized between the knot values. Based on updated parameters, Equation (2.7) is again solved to determine the curve coefficients of the newly fitted curve. Nearest neighbor algorithm requires sampling of the fitted curve in many number of points. For a particular data point, the distance between the data point and each sampled point on the fitted is compared and the sampled point on the fitted curve with the minimum distance is selected.

The employed termination criterion for the overall algorithm is set as the relative change in objective function value between two consecutive iterations. Numerical value for the termination criteria is employed as 1e-6.

2.6 Camber curve construction

Once the profiles of the pressure and the suction sides are reconstructed within the given measurement uncertainty, next, construction of camber curve is accomplished. As described earlier, camber curve construction is required to evaluate the thickness dimension parameters of an airfoil section. Leading edge thickness and trailing edge thickness dimensions are defined at a basic distance from the leading edge point and the trailing edge point respectively. However, maximum thickness dimension occurs in between these dimensions. Therefore, maximum thickness location cannot be detected easily from the measurement points for the evaluation. To determine the maximum thickness, thickness needs to be evaluated along all the points on the camber curve.

2.6.1 Definition of camber curve

Camber curve in airfoil sections is defined as the locus of mid points between the pressure curve and the suction curve such that vector joining two corresponding points on the pressure curve and the suction curve is normal to tangent on their midpoint at the camber curve.
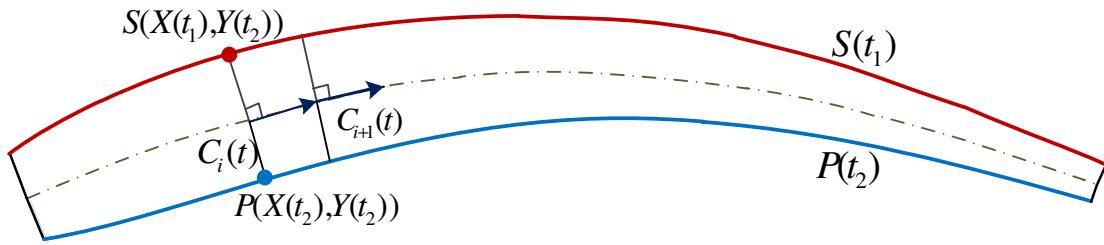
Figure 2.11: Camber curve and its geometric properties

Referring to Figure 2.11, $S(t_1)$ and $P(t_2)$ are the parametric equation of reconstructed curves of the pressure side and the suction side respectively and camber curve is represented by $C(t)$. The geometric properties of camber curve then are represented by following equations:

33

(i) The midpoint property of the camber curve can be represented mathematically as follows:

$$C(x(t)) = \frac{S(X(t_1)) + P(X(t_2))}{2}$$
$$C(y(t)) = \frac{S(Y(t_1)) + P(Y(t_1))}{2}$$

(2.8)

(ii). The scalar product of the vector joining the two corresponding points on the pressure and the suction side and the tangent vector at the corresponding midpoint on the camber curve will be zero.

$$(S(t_1) - P(t_2)) \cdot C' = 0$$

(2.9)

The parameter values t_1 and t_2 characterize two corresponding set of points on pressure and suction sides, such that both the equation are satisfied simultaneously.

2.6.2 Mathematical formulation

In order to determine the points on the camber curve, the parameter values t_1 and t_2 of corresponding point sets on the pressure and the suction sides must be known. If the tangent vector C' at the midpoint of camber curve can be determined, then the Equation (2.9) will have only two parameters t_1 and t_2 to solve for. Furthermore, by employing values of either of t_1 and t_2 parameters, the other parameter can be determined by solving the non linear Equation (2.9). Therefore, tangent determination at the midpoint is required.

The tangent vector C' can be approximated using the numerical method of finite difference. If the points are sampled very close on the camber curve, then approximated tangent will be very close to the theoretical tangent. For estimating the tangent vector at the first midpoint C_1, forward difference method is used which requires the information of the next

consecutive point vector C_2 on the camber curve. C_2 is also the midpoint of next set of corresponding points P_2 and S_2 on the pressure and the suction sides respectively. For approximating the tangent vector at the last point C_n on the camber curve, the backward difference method is used and this will require information of the previous point vector C_{n-1} on the camber curve. The tangent vector on any other point on the camber curve is approximated using central difference method.

Once the information on tangent vectors is available, for a given parameter value t_1, the parameter value t_2 on other curve can be calculated from Equation (2.9). This is to be noted here, parameter value t_2 for all the points on other curve needs to be solved simultaneously as the tangent vectors are approximated based on the neighbour corresponding points. The complete system of equations can be represented mathematically as follows,

$$
\begin{aligned}
(S_1 - P_1).C_1^{'} &= 0 \\
&\vdots \\
(S_n - P_n).C_n^{'} &= 0
\end{aligned}
\tag{2.10}
$$

This formulation in Equation (2.10) represents a system of non linear equations. The determination of parameters is equivalent to the minimization of all the equations simultaneously. An optimization algorithm is employed to minimize this system of equations. The solver tries to approximate each equation to the zero. To initiate the optimization, an initial condition of parameter values is required which is calculated using the nearest neighbour algorithm.

2.7 Case studies

To evaluate the progressive curve fitting algorithm, measurement data points for pressure and suction side curves are simulated and applied to the implemented algorithm. Further, the fitted piecewise curve is examined for closeness with the theoretical curve, using root mean square (RMS) as the closeness measure. Thereafter, camber curve is constructed using the reconstructed curves on the pressure and suction sides and the objective function value on each camber point is examined.

To generate the simulated measurement data points for profile reconstruction, two cases are presented here. The first case considers only measurement error while the second case considers the measurement error with the systematic error on a known curve. Systematic error represents the manufacturing error and is generated by using a sinusoidal function. Thereafter normally distributed values corresponding to a measurement uncertainty are imposed on the simulated measurement error. The generated data points after applying the manufacturing error acts as the manufactured actual curve with which the closeness examination of reconstructed curve is performed.

2.7.1 Profile reconstruction

The first case simulates a situation with only measurement uncertainty. 200 data points are sampled on a single cubic Hermite curve. Normally distributed measurement error corresponding to a measurement uncertainty of $U = 0.01$ is applied on these sampled points. As there is no systematic error therefore, it is expected that during profile reconstruction, single Hermite curve should be able to meet the feasibility condition. The profile reconstruction curve also confirmed this and produced $6\sigma_r = 0.0062$ for a single curve fitting, which is smaller than

the given measurement uncertainty value. Furthermore, closeness of reconstructed curve has also been examined with theoretical actual curve. Root mean square values have been adopted as the closeness measure. Figure 2.12 shows the variation of RMS values with the measurement uncertainty. The increasing trend of graph suggests that as the measurement uncertainty grows, the reconstructed curve lies farther from the theoretical curve.
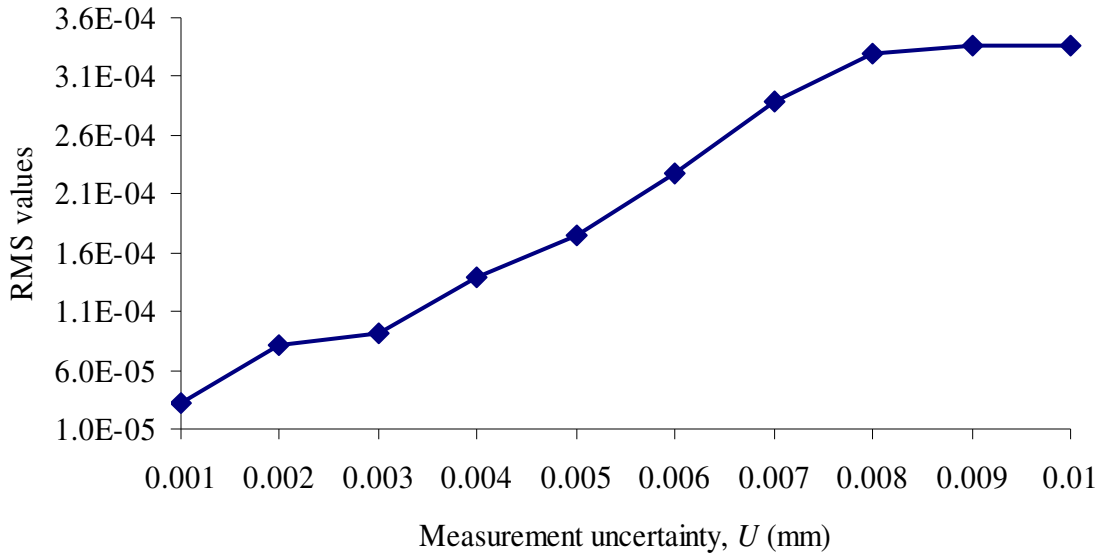
Figure 2.12: RMS deviations of fitted curves with respect to theoretical curve for a case with only measurement error and no systematic error

The second case considers manufacturing error along with the measurement error. 200 points are sampled on the theoretical curve. Thereafter to simulate manufacturing error, sinusoidal function with amplitude of 0.05 mm and 2.5 cycles is employed. The values thus generated are imposed perpendicular to the sampled data points on known curve. Furthermore, normally distributed measurement error corresponding to a measurement uncertainty of $U = 0.01$ is assigned on the generated manufacturing error. Figure 2.13 shows a conformance of progressive curve fitting to the specified feasibility condition. The value of $6\sigma_r$ decreases with increasing number of curve segments in the curve fitting. The specified feasibility condition is met when four Hermite cubic curve segments are employed for fitting.

37
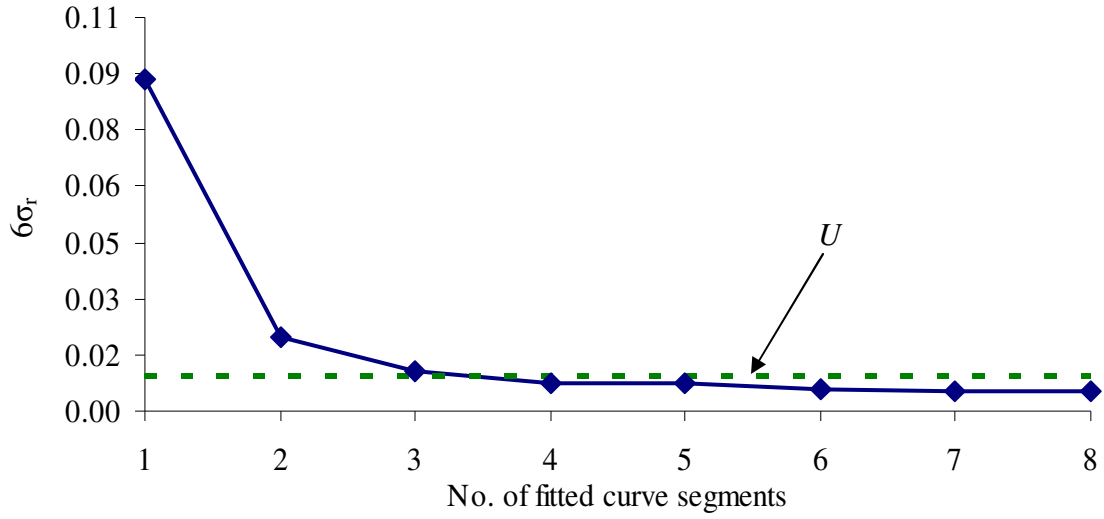
Figure 2.13: Conformance of progressive curve fitting meeting the feasibility condition ($6\sigma_r \leq U$) for the case with systematic error and measurement error

Table 2.1: RMS values between the manufactured curve and the reconstructed curve for varying measurement uncertainty

Applied uncertainty, U	RMS values	No. of curve segments required for fitting
0.001	2.36E-04	7
0.002	2.59E-04	7
0.003	5.26E-04	6
0.004	5.66E-04	6
0.005	1.13E-03	5
0.006	1.17E-03	5
0.007	1.33E-03	4
0.008	1.39E-03	4
0.009	1.41E-03	4
0.01	1.42E-03	4

The closeness of the fitted curve with the simulated manufactured curve has also been examined using RMS value as the closeness measure. Table 2.1 lists the evaluated RMS values between the reconstructed curve and the manufactured curve for varying measurement uncertainty. RMS determines an overall closeness measure. It can be observed from the table that with an increasing U value RMS value increases. The increasing trend confirms the fact that as the measurement uncertainty grows, the probability of accurately approximating the actual curve by a fitted curve reduces.

2.7.2   Camber curve reconstruction

From the fitted curves on pressure and suction sides, camber curve is reconstructed. In the presented case study, two piecewise curves were fitted to the simulated data points for pressure side and three piecewise curves were fitted to the suction side. 51 data points were sampled from the pressure curve and Equation (2.10) was minimized to solve for the parameter values for corresponding 51 points on the suction side. Figure 2.14 shows the reconstructed camber curve. A focused figure shows the input data points on the pressure side and evaluated data points on the suction side. The algorithm also successfully reconstructed for dense input data points.

Furthermore, the value of objective function for each camber point was analyzed. Figure 2.15 shows a plot of objective function values at each data point on the camber curve. To construct a camber curve successfully, it is expected that the value of objective function is zero at each camber point. The figure shows that the objective function value is of the order of 1e-13 for each data point, which means that the solver is able to approximate each equation near zero. Hence, a successful camber curve could be constructed.
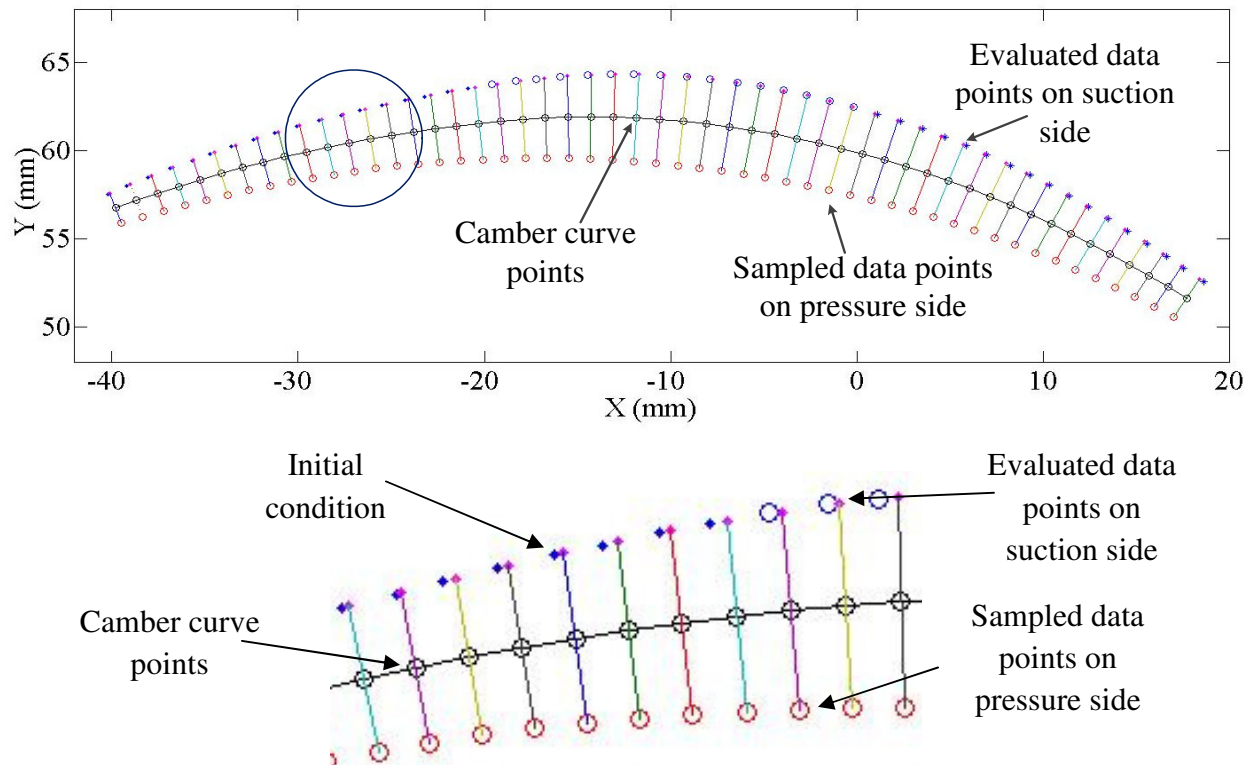
Figure 2.14: Reconstructed camber curve using fitted curves on the pressure and suction side measurement data
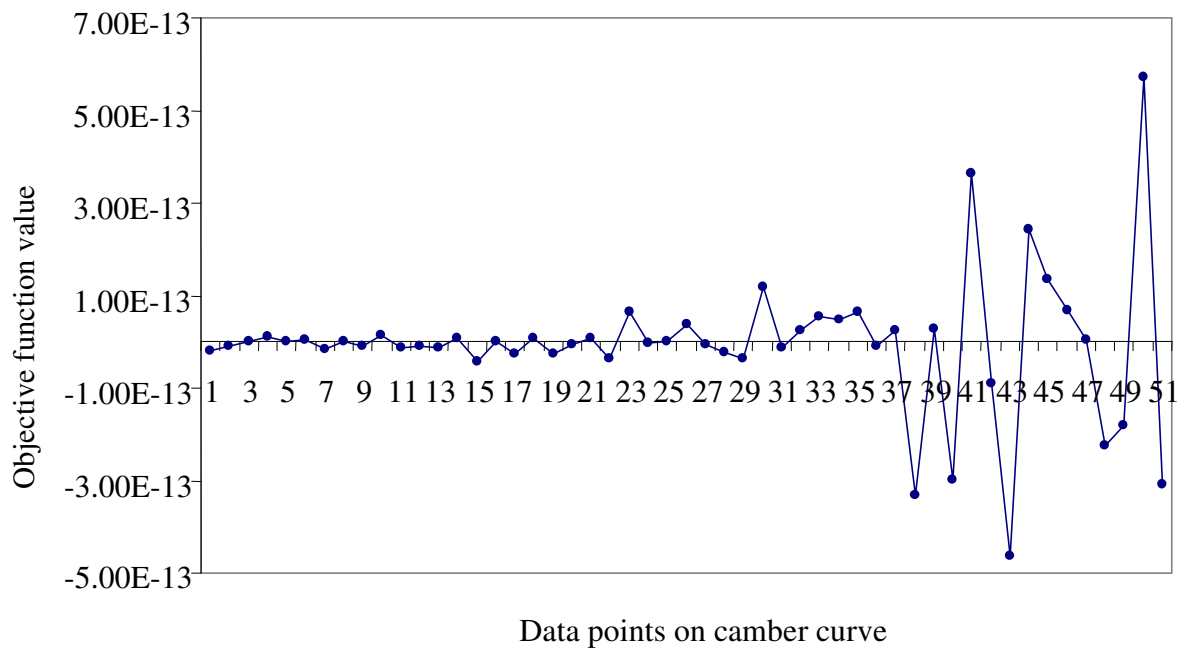
Figure 2.15: Objective function value at every point on reconstructed camber curve

For calculating the thickness dimensions: leading edge thickness, trailing edge thickness and maximum thickness, dense points on camber curve can be generated. Consequently, by evaluating the distance between corresponding points on pressure and suction sides, thickness variation along the camber curve can be determined and thickness dimensions can be evaluated.

3   Profile Tolerance Evaluation

Profile tolerance is a widely used tolerance scheme which represents the allowable geometric variation of a manufactured part surface from its designed surface. Profile tolerance controls simultaneously the form, orientation and sometimes location of the manufactured parts. Profile tolerance can be defined for a single feature in 2D or for a surface in 3D. 3D profile tolerances are generally applied on the components with constant cross sections or parts having continuous revolution. 2D profile tolerances are generally applied to individual features and particularly on those components where, cross sections of part are varying for example: tapered wing of aircraft, impeller blade cross sections [13]. This thesis focuses on the evaluation of profile tolerance for airfoil sections therefore; 2D profile tolerances will be evaluated. Furthermore, during design, the pressure and the suction sides are treated as separate features, hence the profile tolerance evaluation will be performed for them individually.

The subsequent sections in this chapter will discuss in detail profile tolerance definition defined in ASME standard, existing research work in the domain of profile tolerance evaluation. Further, a new methodology for profile tolerance evaluation has been proposed and three case studies are presented to discuss the validity of implemented algorithm.

3.1   Definition

The profile tolerance specifies a uniform boundary along the true profile within which the elements of surface must lie. Profile tolerance zone is created by offsetting the design profile in a normal direction. For a 2D feature, the profile tolerance zone can be imagined as an area while

for 3D surface it will be a volume. The boundaries of tolerance zone follow the geometric shape of true profile.

3.1.1   Classification of profile tolerance

To create the profile tolerance zone boundaries, there are two possible offset directions: inward (inside the material) and outward (outside the material). Based on the offset direction, there are four possible classifications of profile tolerance zone as shown in Figure 3.1.

(i) Bilateral symmetric zone: If profile tolerance value is equally disposed about the true profile in both the directions then it is known as bilateral tolerance zone as shown in Figure 3.1a. Until specified in the drawings, profile tolerance is always assumed to be a bilateral symmetric zone.

(ii) Bilateral asymmetric zone: If profile tolerance value is unequally disposed about the true profile in both the directions then it is known as bilateral asymmetric tolerance zone as shown in Figure 3.1b In case of unequally disposed bilateral tolerances, it is necessary to show the split of tolerance zone about the nominal in the drawing.

(iii) Outside unilateral zone: If complete zone lies outside of the true profile then it is called unilateral profile tolerance zone as shown in Figure 3.1c.

(iv) Inside unilateral zone: If complete zone lies inside of the true profile then it is called as unilateral profile tolerance zone as shown in Figure 3.1d.
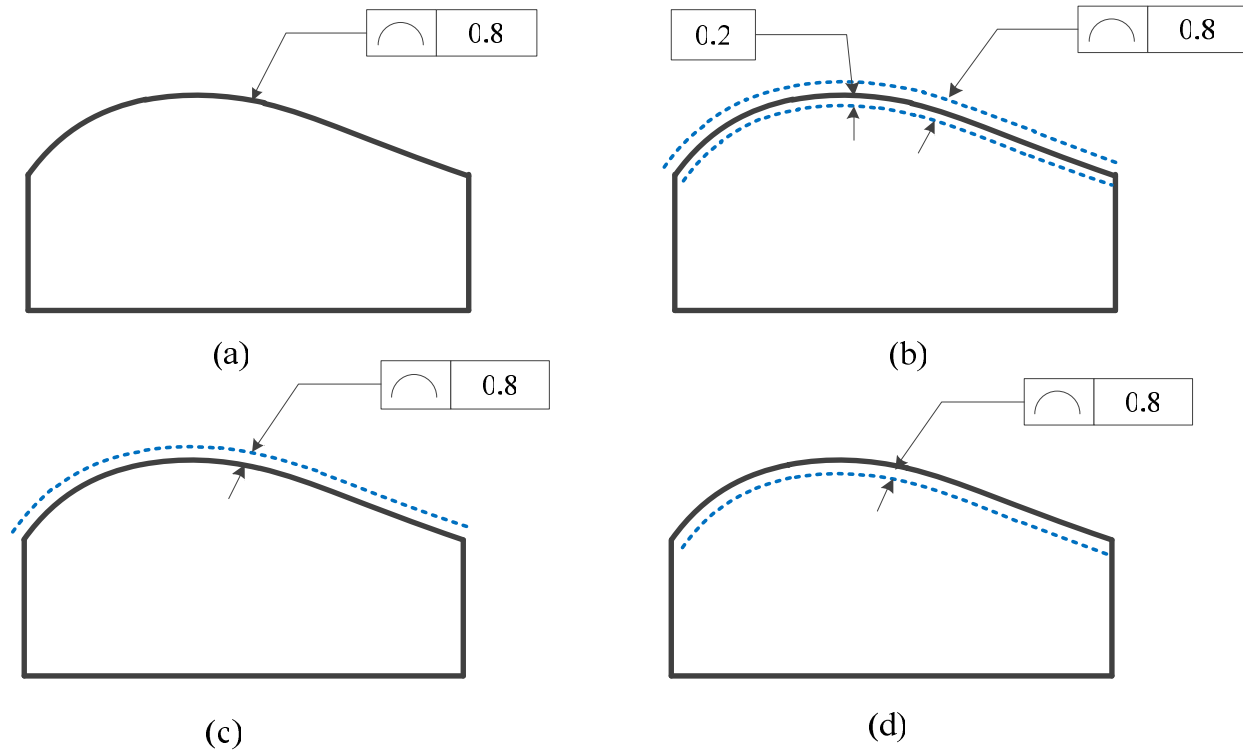
Figure 3.1: Profile tolerance classification: (a) Bilateral symmetric (b) Bilateral asymmetric (c) Outside unilateral (d) Inside unilateral. The firm line shows nominal curve and dotted lines represent specified tolerance zone boundaries [13]

3.1.2 Conformance and actual value

Quality inspection of a manufactured surface requires the comparison of the data points acquired by CMM with the specified design tolerances of the target geometry. The task of tolerance verification is characterized into two aspects: (i) determining the conformance (ii) and the minimum zone evaluation [14]. Conformance concerns whether a manufactured part meets the design tolerance specification or not. To meet the conformance criterion, all the measurement data points inspected on the surface of manufactured part should lie inside the specified tolerance bounds. The actual profile boundary is defined by the maximum deviation of CMM points from the nominal design profile on both the sides.

The second aspect determines how well the manufactured part meets the design tolerance specifications. It examines if the manufactured part just fits in the tolerance zone or if there is ample space remaining inside the tolerance zone. This quantitative characterization is useful in estimating the process capability. This quantitative characterization is determined based on the concept of minimum zone. Therefore, as shown in Figure 3.2, the aim of profile tolerance evaluation is to determine the minimum zone value formed by the measurement data points about the nominal and check the conformance of evaluated tolerance boundaries with specified tolerance bounds. The part is accepted if the evaluated boundaries lie inside the specified tolerance bounds otherwise it is rejected.
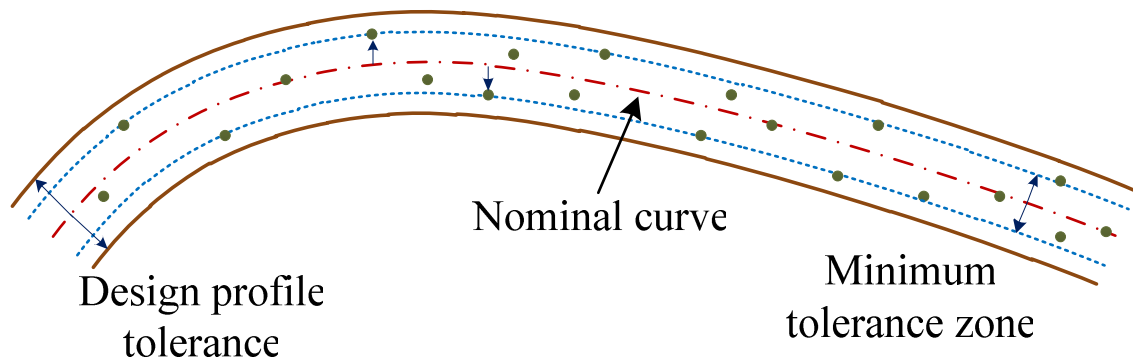
Figure 3.2: Specified profile tolerance zone and the minimum zone formed by measurement data points on the nominal curve

3.2   Existing algorithms

The coordinate measurement of an object's surface provides discrete data points. These data points are measured in a measurement coordinate system (MCS), which is different from the design coordinate system (DCS) in which the design geometry lies. Therefore, for associating the measurement data points with the nominal profile, generally, numerical fitting approaches are employed. Numerical fitting methods locate the measurement data points onto the design

geometry by using a rigid body transformation. To determine this transformation, the translation and rotational parameters are needed to be determined. Due to the manufacturing set-up errors and form errors, the measurement points do not exactly replicate the design geometry. Therefore, the determination of transformation parameters is basically an optimization problem [18]. The criterion of optimization depends on the measure of closeness between the data points and design geometry. Currently available measures are mainly categorized into least square fitting, minimax fitting, and zone fitting. These methods are being described in detail in the following section.

3.2.1 Least square fitting

This is one of the most popular fitting algorithms for CMM data inspection analysis. It minimizes the sum of squares of the deviations to determine the optimal parameters which places the CMM data points with respect to the design geometry. The deviation is calculated as the shortest distance between the CMM data point and the nominal curve. The mathematical formulation of least square fitting is represented as follows,

$$Obj\_fun = \min(\sum_{i}^{n} e_i^2) \tag{3.1}$$

where, e_i is the deviation between CMM inspection point M_i and the nominal curve. The deviation e_i is dependent on the transformation parameters and nominal curve parameters. In case of a line or a plane, this formulation can be converted to linear least square problem, for which a solution is readily available. However, in case of freeform curves or polynomials, this problem becomes nonlinear and hence is usually solved iteratively [18].

The solution of least square fitting passes through the sample mean of normal distribution of deviations. This fitting minimizes the overall root mean square error but may increase the

maximum deviation. Hence it tends to overestimate the tolerance values and as a result it can reject the acceptable parts [23]. Menq [16] used this fitting for surface profile inspection. Furthermore, Murthy and Abdin [17] showed that a least square fit may not always give the minimum zone deviation.

3.2.2 Minimax fitting

The least square fitting tends to minimize the root mean square error however, it may increase the maximum deviation, therefore there is an inconsistency between the tolerance definition in the ASME standard and the least square concept. Therefore, an alternate method minimax fitting was developed [23]. Minimax fitting finds the optimal parameters such that the maximum deviation between the measured data set and true profile is minimized. It is also known as two sided minimax fitting [15]. The problem is formulized as following:

$$Obj\_fun = \min(\max_{1 \leq i \leq n}|e_i|) \tag{3.2}$$

This is also known as L_∞ norm problem. Minimax fitting is suitable for estimating roundness, cylindricity and flatness. Minimax fitting suffers with the numerical instabilities as the first derivative of objective function is not continuous. Hence, there have been various attempts to avoid the numerical difficulties of this formulation. Murthy and Abdin [17] used Monte Carlo technique based on the downhill simplex search and the spiral search technique to evaluate the minimum zone. They also showed that the minimum zone obtained in this manner is smaller than the least square fitting. Wang [20] also formulated the problem as nonlinear constrained optimization. Etesami and Qiao [21] used convex hull approach instead of optimization. Since the approach is based on computational geometry, their algorithm determines exact answer. Carr

and Ferreira [22] proposed various form tolerance evaluation algorithms for flatness, straightness and cylindricity. In their approach, they converted the minimax problem into a series of linear programs. With proper and enough initial conditions, the local minimum solution determines the minimum zone solution. Minimax fitting minimizes the largest deviation; hence it gives the tightest fit tolerance. But this may lead to an overall higher root mean square error. In some cases it is possible that minimax fit results in acceptance of bad parts [23].

3.2.3   Zone fitting

Identifying the shortcomings of previous two approaches, Choi and Kurfess [18] suggested a zone fitting approach. They considered the tolerance zone as geometric bounds and argued that it is not necessary to determine the deviation from nominal for the conformance with the specified tolerance bounds. Instead, a transformation vector can be found to see if the measurement data points lie inside the bounds or not. Figure 3.3 illustrates the zone fitting method for a 3D profile tolerance zone. They formulated zone fitting problem as a truncated least square problem in which the residual of a CMM point becomes zero, when the point lies inside the tolerance zone. Hence, when objective function value becomes zero, then all the measurement points will lie inside the tolerance zone. However, zone fitting problem only gives information on the conformance or non conformance of a surface with the design limits and cannot evaluate the minimum zone.

Choi and Kurfess [19] further extended their work of zone fitting method to calculate the minimum zone using an iterative approach between the zone fitting and the bisection root finding method. In this paper, using bisection search method, the boundaries of tolerance zone were updated (shrunk or expanded) and every time, updated boundaries were tested with the zone

fitting method. Choi and Kurfess [19], implemented this algorithm to determine the flatness, cylindricity and roundness. The zone fitting approach has further been utilized by Qian and Yang [23] to calculate the exact volume of tolerance zone space. They utilized the truncated average fit model for the data localization which utilized the average distance of points outside the tolerance zone for objective function.
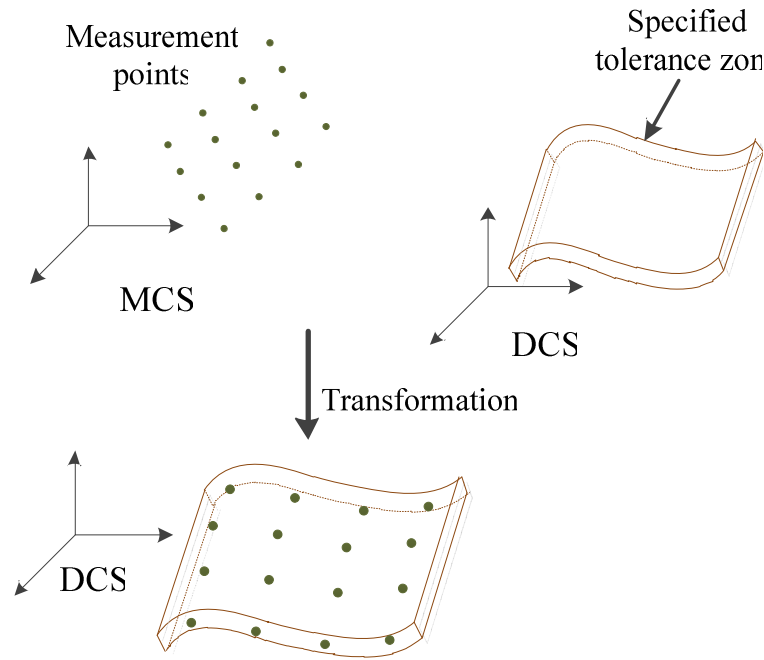
Figure 3.3: Zone fitting method transforms the measurement data points (in MCS) within the specified tolerance zone (in DCS) [18]

3.3 Proposed method of scaled minimax

3.3.1 Scope for new method development

The existing methods of fitting are not versatile in nature as they cannot deal with all the three types of profile tolerances namely: bilateral symmetric, bilateral asymmetric and unilateral tolerance. As described earlier in section 3.1.2, one of the tasks of tolerance evaluation is the conformance of manufactured part deviation with the specified tolerance boundaries. Therefore,

the measurement data should fit directly in the specified tolerance zone. In order to conform to the design tolerance limits, the deviation of error zone, on inner and outer side of the material should be smaller or equal to the corresponding tolerance limits. The earlier described method of least square fitting tends to overestimate the maximum deviation. The least square fitting method is suitable for the situations when, measurement data points are interpreted as sampled data points from unknown surface, as this fitting gives the maximum likelihood solution [23]. However, least square fitting is not applicable to all types of profile tolerances. This is evident for unilateral case, as the zone produced by least square fitting will never conform to the design boundaries of unilateral zone.

Minimax fitting is closer to the standard definition of profile tolerance. However it is only applicable to the bilateral symmetric tolerance as the produced zone is always symmetric. For evaluating unilateral tolerances, minimax fitting can be formulated as one sided minimax fitting with constraints on the residuals such that they are always inside or outside of nominal [15]. However minimax fitting cannot confirm to the asymmetric tolerance zones.

Zone fitting is a more versatile approach as it tries to place the points inside the design tolerance boundaries. Therefore, it can be used for conformance of all type of profile tolerances. However, in order to determine the minimum zone, this method iterates between the estimation of tolerance boundaries and zone fitting. Therefore, determining the minimum zone using zone fitting is a multi step method.

The study of current fitting methods suggests that there is a scope for the development of a single step and unified method which can conform to all types of profile tolerance definitions

and as well as can evaluate the minimum zone without multiple step estimation of tolerance boundaries.

3.3.2 Methodology

A novel method of 'scaled minimax' is devised here to achieve the above stated objective of a single step unified tolerance evaluation. The method is built on the minimax fitting concept so that the method remains more consistent with the standard tolerance definition. The main concept behind the scaled minimax algorithm is based on the fact that by employing a user specified constant S during the formulation of objective function, relative position of evaluated tolerance boundaries can be controlled. If the residuals of data points located on the inner side of nominal geometry are scaled by this constant, then after minimax fitting, the resulting maximum residuals on outer and inner side will be in the ratio of S. This should be noted here, that only for minimization, residuals are being scaled. This does not scale their actual position.

To further elaborate on this minimax fitting has been recalled here. Minimax fitting minimizes the maximum of the residuals of the data points. It is well known, that when the maximum deviation is minimized, the maximum residual on each side will be becomes equal. To demonstrate the scaled minimax concept mathematically, let the initial residuals on outer side and inner side of nominal curve be denoted as r_{outer} and r_{inner} respectively. The residuals on inner side are scaled by the specified scaling constant S as follows:

$$e_i = \begin{cases} \left| r_{outer} \right| & if \quad r \geq 0 \\ S \times \left| r_{inner} \right| & if \quad r < 0 \end{cases} \tag{3.3}$$

The minimax fitting algorithm will consider the absolute maximum error for minimization. Hence,

$$Obj\_fun = \min(Max(|e_i|))$$

(3.4)

As described earlier, when the minimum objective function is attained in minimax fitting, the maximum error on each side will be equal. Hence,

$$\max(e_{outer}) = \max(e_{inner}) \qquad (3.5)$$

By substituting the corresponding residual values in Equation (3.5),

$$\max(r_{outer}) = S \times \max(r_{inner}) \qquad (3.6)$$

here, maximum of the residuals on outer side and inner side defines the boundaries of minimum zone and it is evident from Equation (3.6), that evaluated boundaries are in the user specified ratio S.

The constant can be assigned by the manufacturer, depending on their process capability requirements. One logical selection of constant will be to consider it as a ratio of outer and inner tolerance boundary as this value of ratio will enable the positioning of error zone boundaries in proportion to their allocated budget in design.

$$S = \frac{D_{out}}{D_{in}} \qquad (3.7)$$

where, D_{out} and D_{in} are the specified tolerance boundaries.
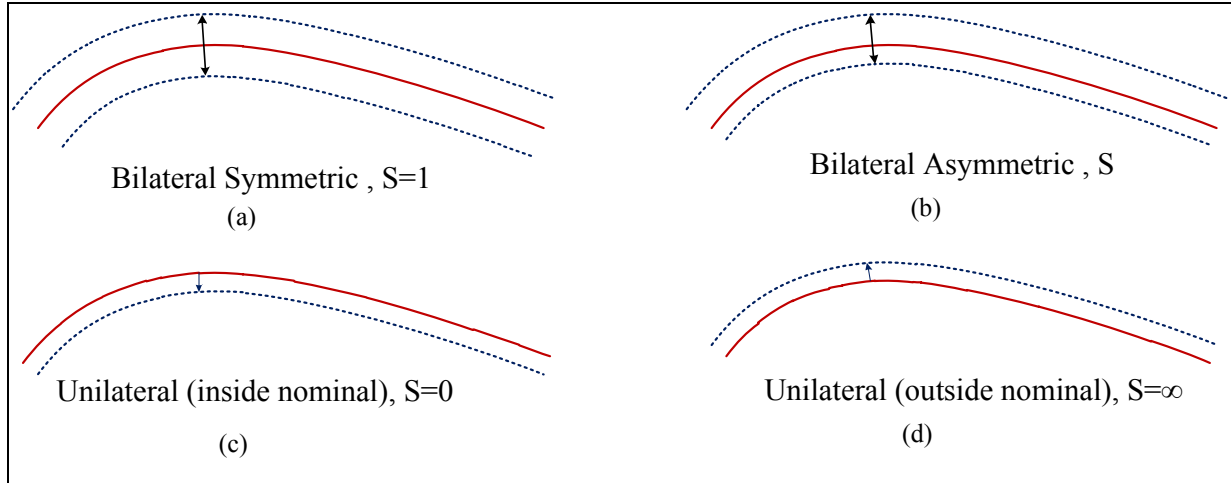
Figure 3.4: Scaling constant for different types of profile tolerances

As shown in Figure 3.4, for bilateral symmetric case the user specified constant will become '1', and therefore, scaled minimax fitting will translate to standard minimax fitting. Unilateral case in which specified tolerance boundary lies on the inner side of the nominal, the value of specified constant becomes '0'. And due to scaling of residuals, the points on inner side of material will not contribute to the maximum error selection. Therefore during minimization, points located in outer zone will be forced to move towards the nominal profile till there is no point on the outer side and atleast one point touch the nominal profile. Likewise, unilateral case where specified tolerance boundary is on outer side of nominal, the value of specified constant becomes '∞'. In this situation, the constant magnifies the magnitude of residuals on inner side; hence during minimization, algorithm will force the points in the inner zone towards the nominal profile until all the points are placed on the outer side of nominal.

For bilateral asymmetric case, this specified constant enables the minimization of error zone boundaries in proportion to the tolerance boundaries. It is evident that the scaled minimax method can address all types of profile error evaluation and can also evaluate the minimum zone without any error boundary estimation.

3.4   Detailed procedure

To determine the transformation parameters which can locate the measurements onto the nominal geometry, a set of corresponding points on the nominal geometry are required. Therefore, there are two sets of unknowns for optimally positioning the measurement data points with respect to the nominal geometry: curve corresponding points and transformation parameters. The overall problem of minimizing the objective function is solved in two iterative steps. First assuming corresponding points are given, transformation parameters are determined to minimize the overall objective function. In second step, corresponding points are established. The process is iterative till a stopping criterion is met.

The overall flow chart for scaled minimax algorithm is described in Figure 3.5 . To initialize the optimization, the curve corresponding points are established by uniformly sampling the data points on the nominal curve. The following sub sections will describe the key steps in detail.
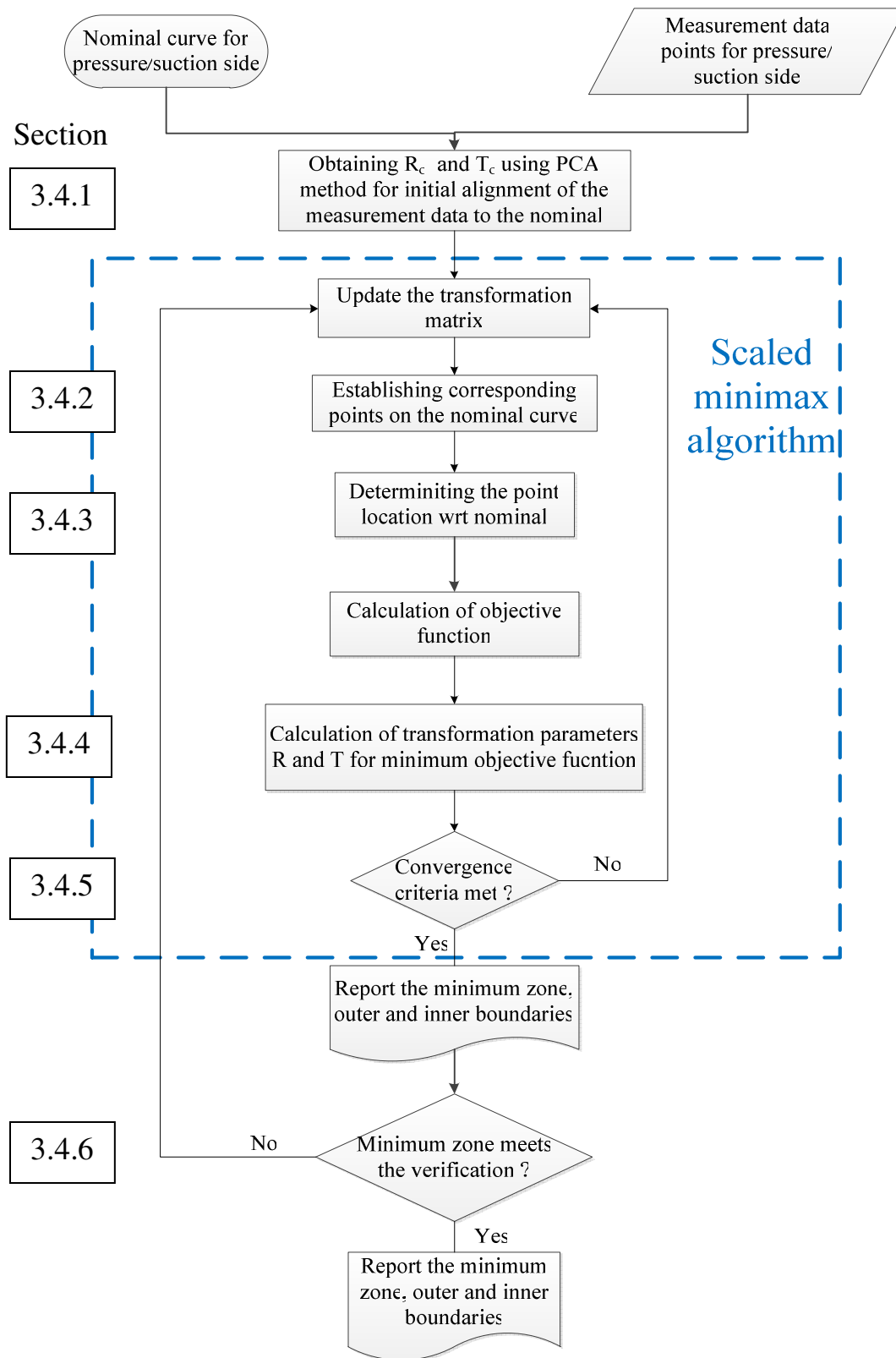
Figure 3.5: Flowchart for profile tolerance evaluation

3.4.1　Initial alignment using PCA

The initial alignment is required as the data points are measured in a different coordinate system than the design coordinate system. Therefore, it is possible that there is a significant variation in the measurement data and the design curve. This may increase the errors between the nominal curve and the measurement data set and further fail to obtain the optimal fitting [6]. This work uses method of principal component analysis (PCA) for determining the initial rotation matrix R_o and T_o. PCA method is based on using the direction of the main axis of the area formed by the cluster of points. If the overlapping region between the data points and the sampled points on the nominal curve is large enough then both main axis will be almost coincident. The main axes are determined by calculating the Eigen values and Eigen vectors of the covariance matrix of each data set. The pressure and suction side curves are generally smooth therefore PCA method can be employed without any difficulty. PCA method is a computationally efficient method [24] and reasonably aligns the data points on the nominal geometry. The data points are positioned with respect to the nominal geometry based on the transformation matrix calculated from PCA method. For further optimal fitting, an identity matrix is used as an initial condition. PCA method has an established mathematical formulation and it has adopted here in this thesis work.

3.4.2　Corresponding point determination

Once the measurement data points are initially aligned with the nominal geometry, a new set of corresponding points need to be re-established, as the earlier selection of corresponding points was arbitrary. The corresponding points are established based on the closest point concept, which in this case is the foot point of perpendicular drawn from the measurement point.

In practice, nominal curve for airfoil sections are designed as either cubic degree or higher degree curves [6]. Hence, there is no close form solution available for determining the corresponding point parameter and it needs to be solved iteratively. As mentioned in Chapter 1 section 1.4, for the implementation of method, a cubic degree Hermite curve is assumed for simple calculations.

Figure 3.6: Determination of a corresponding point on the nominal curve to a measurement data point

In Figure 3.6, let CMM point M_i have coordinates (x, y) and the corresponding point on CAD curve be $S(t)$ with coordinates $(X(t), Y(t))$. Then the distance between these two points is given by,

$$distance = (X(t) - x)^2 + (Y(t) - y)^2 \tag{3.11}$$

For a closest point criterion, this distance will be differentiated with respect to parameter t, such that the distance minimizes. Hence differentiating Equation 3.11 wrt t,

$$2(X(t) - x)X^{'}(t) + 2(Y(t) - y)Y^{'}(t) = 0 \tag{3.12}$$

Equation (3.12) gives a fifth degree polynomial in t; hence, an exact solution cannot be calculated. To determine an approximated solution, an initial guess is required, which is calculated using nearest neighbour algorithm. For minimization of the Equation (3.12), *Fzero* function of MATLAB is being utilized, which uses a combination of bisection, secant and

inverse quadratic interpolation methods. Minimization function utilizes the initial guess and iterates until the equation value becomes zero or approximates zero. After minimization, the function returns parameter value t_o for the corresponding point. And by substituting it in the nominal curve equation, the corresponding point can be calculated. Similar procedure is followed for determining the corresponding point to each measurement data point.

3.4.3 Point location determination

To formulate the objective function, deviation of data points on outer and inner side of the nominal needs to be known. For this, first location of measurement data points needs to be categorized in outer and inner. The principle behind 'point location' determination is the resultant direction of the cross product between two vectors. The first vector joins the corresponding point to the measurement data point and the second vector is the tangent vector on the nominal curve at corresponding point.

As shown in Figure 3.7 the clockwise rotation of a vector is considered positive and counter-clockwise rotation is considered negative in the implementation. Hence, if a measurement point lies on the outer side of nominal, then the vector joining this data point and curve corresponding point, towards the tangent vector on the nominal curve will be clockwise, while if the point lies on inner side of curve, then this rotation will be counter clock wise. Hence, these measurement data points can be easily classified into outwardly located or inwardly located.
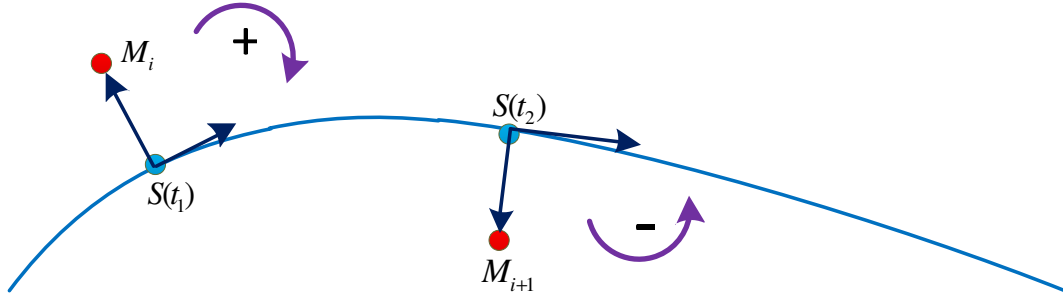
Figure 3.7: Determination of point location with respect to nominal curve

The point to be noted here is that during determination of transformation parameter for minimum objective function, the corresponding points remain fixed. However, the position of measurement points changes as the transformation parameters are varying. Therefore, it is necessary to recalculate the corresponding points for the point location determination. The corresponding points are updated to avoid any anomaly resulting due to the convex nature of nominal curves.

3.4.4 Minimization using downhill simplex search

After the location determination of the data points, residual for each data point can be calculated. The scaling factor is employed to the residuals belonging to the points on inner side. After scaling, maximum of the residual is calculated as objective function. Once the objective function is formulated, the next task is to search for the transformation parameters which can minimize the objective function. The formulated objective function is non smooth in nature as the first derivative of the objective function is non differentiable [18]. Therefore, the standard methods of minimization such as Quasi Newton or any other gradient based method cannot be used as they require first and higher derivative calculation. To minimize such non differentiable functions, direct search techniques are very popular [27]. These methods do not require any

gradient information. Instead they search many neighborhood points around the current point and look for a point where the objective function value is lesser than the current value.

One of the very popular direct search methods is Downhill simplex search method [32]. Downhill simplex search algorithm starts with the construction of a simplex of $z+1$ dimensions in the search space of z dimensions. In the current case, as the search space is three dimensional (for *x*-translation, *y*-translation and rotation in *x-y* plane); therefore, a simplex of tetrahedron shape will be created around the initial condition. The method initiates with the ordering of vertices of simplex in the decreasing order of objective function value. The basic idea is to replace the vertices with highest objective function value by another point with a lesser objective function value. The method involves key steps of expansion, reflection, contraction, and shrinkage. The search is performed until the diameter of simplex is smaller than a specified tolerance. For implementation, *Fminsearch* solver of MATLAB has been used. This solver is a modified version of basic downhill simplex search method.

3.4.5   Convergence criteria

The iterative process of corresponding point determination and transformation parameter calculation is performed till the calculated convergence criterion is smaller than the assigned tolerance. The convergence criterion is set here as the relative change in the value of objective function in two consecutive iterations and the assigned tolerance is set as $1e-6$.

3.4.6   Verification of objective function value

As mentioned in section 3.4.4, the objective function formulation is nonlinear and as well as non differentiable in nature hence, it is expected to have multiple locals. Direct search method

can deal with optimization of such formulations; however, they are known to give local solutions [27]. Therefore, a verification of the achieved solution from the scaled minimax method is recommended. The verification method will verify whether the achieved solution is the minimum possible solution or if it is a local solution. A good candidate for the verification method is the zone fitting method as it can verify against the specified boundaries. Furthermore, as Choi and Kurfess [18] suggested the form of zone fitting objective function is smooth in nature, therefore it is expected to converge to a global solution provided a good initial condition is there. In the present case of scaled minimax, the transformation parameters for an already converged solution acts as a good initial condition for the zone fitting method.

The zone fitting method tries to place the measurement data points inside the specified tolerance bounds. In order to use the zone fitting method as a verification tool, the currently evaluated boundaries from scaled minimax method are decreased by a pre-specified amount. This pre-specified amount is termed as resolution in this thesis work. Thereafter, zone fitting method tries to place the measurement points inside the updated tolerance boundaries. For initial condition, zone fitting method utilizes the transformation parameters corresponding to the converged solution of scaled minimax. The zone fitting method succeeds if the points are placed inside the updated tolerance bounds. This suggests that there is further smaller zone available and the solver for scaled minimax got stuck in the local minima. Thereafter, to further minimize the objective function of scaled minimax algorithm; the transformation parameters obtained from the zone fitting method are used as an initial condition to the scaled minimax method. The process of determining the solution using scaled minimax and verification with zone fitting method is iterative in nature and is performed, until a zone is confirmed by the verification

method. Brief information on the zone fitting method's mathematical formulation and it's use as a verification tool is discussed here.

Let the tolerance boundaries of the obtained solution from the scaled minimax method be E_{out} and E_{in}. For zone fitting, these boundaries are reduced by a pre-specified resolution amount and such that the ratio of produced boundaries obliges the scaling constant S. The resolution is selected as 0.01%. Hence, the boundaries for zone fitting will be as following,

$$
\begin{aligned}
E_{out}' &= E_{out} \times (1 - resolution) \\
E_{in}' &= E_{in} \times (1 - resolution)
\end{aligned}
\tag{3.13}
$$

where, E_{out}' and E_{in}' represents the updated tolerance bounds. The zone fitting algorithm uses a truncated least square objective function which is defined as follows:

$$
Obj_{zone\_fitting} = \sum_{i=1}^{n} r_i^2
\tag{3.14}
$$

where,

$$
r_i = \begin{cases}
(dist(m,S) - E_{out}')^2 & if \quad E_{out}' \leq dist(m,S) \\
0 & if \ E_{in}' \leq dist(m,S) \leq E_{out}' \\
(dist(m,S) - E_{in}')^2 & if \quad dist(m,S) \leq E_{in}'
\end{cases}
\tag{3.15}
$$

here, $dist(m,S)$ is the normal deviation between the measurement point M_i and the nominal curve. This quantity is a function of transformation parameters (t_x, t_y, θ). Hence minimization of this objective function is an optimization problem. Equation (3.15) suggests that the minimum possible value of objective function is zero. Therefore, when zone fitting succeeds, then the objective function value will become zero. A non-zero objective function value will suggest that zone fitting could not place the points inside the updated tolerance bounds.

62

3.5 Case studies

The implemented algorithm has been tested on more than 75 different simulated data sets. The algorithm successfully demonstrated the versatility of algorithm for bilateral symmetric, bilateral asymmetric and unilateral profile tolerances. Three representative case studies are presented in this section. The first case study discusses a case which shows that scaled minimax algorithm is more consistent with bilateral asymmetric type profile tolerance evaluation in comparison to the minimax algorithm. The second case study is focused on the examination of the form of scaled minimax objective function formulation. And the last case study discusses the effectiveness of the verification module and its impact on improving the minimum solution.

3.5.1 Data set design and validation of solution

For the study of algorithm, the measurement data sets were simulated by superimposing the normally distributed noise corresponding to a manufacturing error on the nominal design. The values were always assigned to the points in a direction normal to the curve. As the generated noise always has a positive and negative bound. Therefore, the simulated data points create an outer and inner boundary about the nominal, which is treated as the initial zone. The generated data points were further transformed by using an initial transformation (t_x, t_y, θ) to provide a similar situation as for the inconsistency between the coordinate systems of inspection and design. Figure 3.8 represents a typical simulated case study. The figure shows the nominal profile and the generated measurement data set corresponding to a normal distribution with spread value (6σ) of 0.5. The data set for presented case studies is also simulated in a similar way for different values of noise and transformation vector (t_x, t_y, θ). Using the proposed

algorithm, the measurement data set is optimally fitted on the nominal curve and evaluated zone value is compared with the initial zone value.
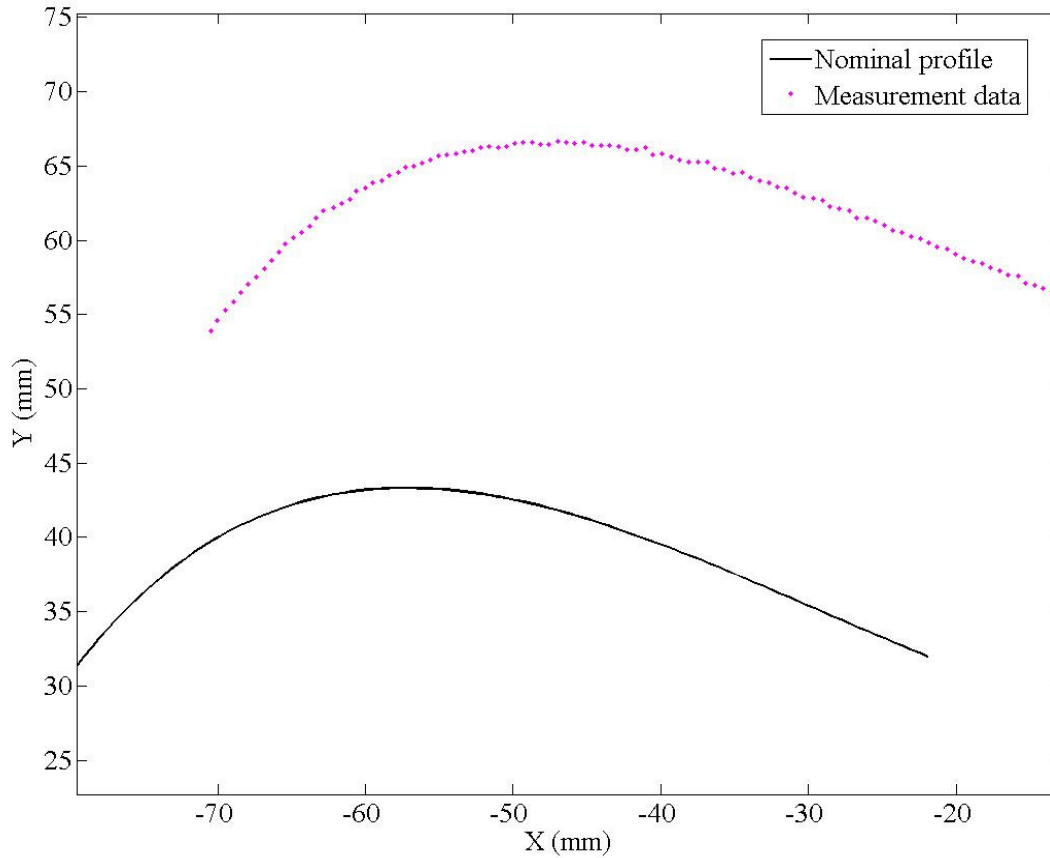
Figure 3.8: Typical simulated case study shows the measurement data points and the nominal profile

The important point to note here is that, there is no theoretical zone, to which the evaluated zone can be verified with. However, the initial zone value is one of the solutions for given data points. Therefore, it is expected that the zone evaluated by the profile tolerance algorithm should be either equal to or smaller than the initial zone.

3.5.2 Case study 1: Usefulness of scaled minimax method over minimax method

The first case study compares the scaled minimax fitting with the minimax fitting for a bilateral asymmetric profile tolerance case. It is known that minimax algorithm will always give symmetric tolerance boundaries. Therefore, in case of bilateral asymmetric tolerance evaluation, there is a possibility that the evaluated zone boundary by minimax does not confirm to the specified tolerance boundaries. The basic parameters for case study design are mentioned in Table 3.1. In this case, the specified tolerance boundaries are assumed to be the outer and inner boundaries of the initial zone. As shown in Table 3.2 , the outer and inner boundaries of initial zone are not equal. Therefore, the value of specified constant S is not 1 and the case has become a bilateral asymmetric tolerance evaluation. This predetermined selection of S ensures that the boundaries of the evaluated zone from scaled minimax lies inside the initial zone.

Table 3.1: Design parameter for case study 1

No of points, n	199
Manufacturing error (6σ)	5.00E-04
Initial transformation vector $(t_x(mm), t_y(mm), \theta(radian))$	10, 25, 1.00E-04
Scaling constant, S	1.21

Table 3.2: Outer and inner boundaries of evaluated zone using Scaled minimax and Minimax method for Bilateral asymmetric case. All values in mm

	Initial zone	Scaled minimax	Minimax
Outer boundary	2.98E-04	2.89E-04	2.65E-04
Inner boundary	2.45E-04	2.38E-04	2.65E-04
Zone value	5.44E-04	5.27E-04	5.31E-04

Table 3.2 shows the evaluated results for both the scaled minimax and the minimax method. The zone value for both algorithms is smaller than the initial zone value, which signifies that the algorithm is converging properly. For scaled minimax case, both the outer and inner boundaries of evaluated zone are lying inside the initial zone boundaries. While for the minimax fitting, the inner boundary of the evaluated zone exceeds the inner boundary of the initial zone and thus, minimax fitting does not confirm to the specified tolerance boundaries. This signifies that for bilateral asymmetric tolerance evaluation, scaled minimax method is more consistent with the zone conformance criterion than the minimax method.

3.5.3 Case study 2: Form of the objective function

Case 2 studies the form of the objective function of proposed method. It has been discussed before that the partial derivatives of minimax function are discontinuous in nature and it is expected to have multiple local minimum. Therefore, it is useful to investigate the form of objective function to check, if the achieved solution is a local solution or a global one. Table 3.3 lists the basic parameter of case study 2.

Table 3.3: Design parameter for case study 2

No of points, n	199
Manufacturing error (6σ)	6.00E-04
Initial transformation vector $(t_x(mm), t_y(mm), \theta(radian))$	10,25,0.05
Scaling constant, S	1.3

Table 3.4 : Transformation parameters and objective function value for converged solution of Scaled minimax method

	T_x	T_y	Theta	Obj Fun
S1	-2.09E-04	-1.48E-04	-2.97E-06	3.33E-04

66

The implemented algorithm is tested on the simulated data set of case study 2. Table 3.4 lists the transformation parameters and the objective function value for converged solution from the scaled minimax algorithm. Further, the objective function was plotted near the achieved solution. As there are three transformation parameters therefore the function cannot be plotted for all of them. Hence, T_x is kept fixed and objective function is plotted for a varied T_y and *Theta*. Figure 3.9 shows the $x - z$ perspective of the plot. As the plot shows, the objective function form is irregular near the solution. A focused view of highlighted section is also shown. The plot confirms that the objective function has multiple local minimum. The achieved solution *S1* is also a local solution and the initial condition from PCA method is not able to give the global minimum solution. The decreasing trend of objective function also suggests that the objective function value can be further minimized. Therefore, there is a need of a supplement method which can verify the solution of scaled minimax as a local or a final solution. Zone fitting is adopted as the verification method here. Zone fitting method not only verifies the solution and but also provides a transformation parameter vector for further minimization. The next case study focuses on the effectiveness of verification method.
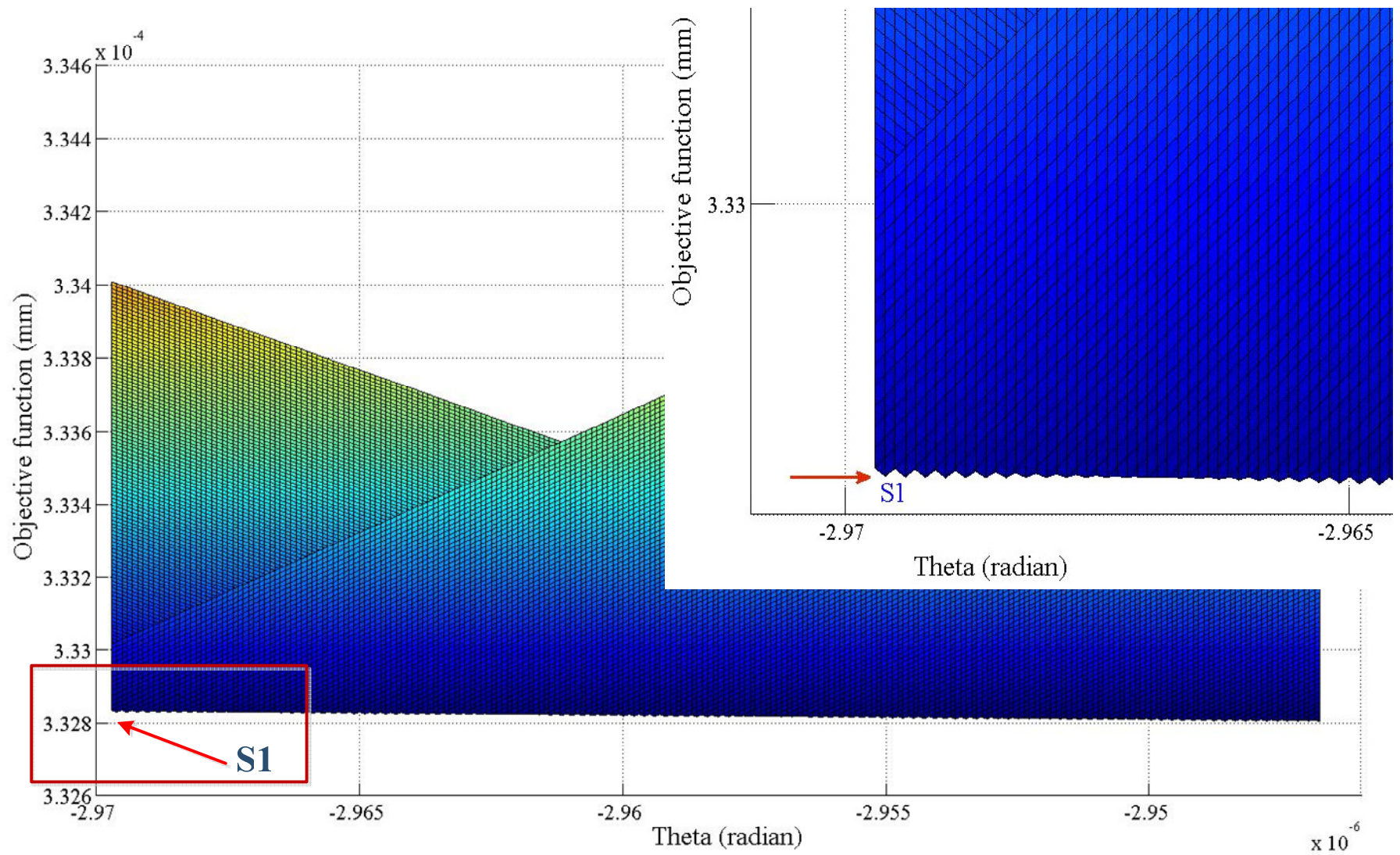
Figure 3.9 : x-z perspective of a 3D plot of objective function form for case study -2. The objective function is irregular near the solution. The converged solution S1 is local in nature.

3.5.4   Case study 3: Effectiveness of verification module

The case study 3 studies the effectiveness of verification module. As the objective function has multiple minima therefore it is expected that verification method should be able identify the locally converged solution of scaled minimax method. Two case studies are presented under this section.

(i) The verification module is tested on the simulated data set of case study 2. The transformation parameters and corresponding objective function for each converged solution for scaled minimax are listed in the Table 3.4 **.** The table also lists the transformation parameters achieved from the verification module corresponding to each converged solution of scaled minimax.

Table 3.5: Transformation parameters for scaled minimax method and the verification method for each local solution (Case study-2)

	Scaled minimax method				Verification method			
	Tx	Ty	Theta	Obj Fun	Tx	Ty	Theta	Obj Fun
S1	-2.09E-04	-1.48E-04	-2.97E-06	3.329E-04	-2.10E-04	-1.48E-04	-2.98E-06	0
S2	-2.10E-04	-1.48E-04	-2.98E-06	3.328E-04	-2.10E-04	-1.47E-04	-2.95E-06	0
S3	-2.10E-04	-1.47E-04	-2.95E-06	3.328E-04	-2.11E-04	-1.46E-04	-2.94E-06	4.77E-16

From the form of objective function in case study 2, it is already known that the solution *S1* is a local solution. Table 3.5 suggests that verification method is able to identify it as the corresponding objective function value is 'zero'. Recalling zone fitting objective function form, when the points are placed inside the zone boundaries, then objective function value becomes zero. The transformation parameters produced by the verification method corresponding to solution *S1* are then used as initial condition for scaled minimax. If the achieved solution *S2* is checked again in the objective function plot Figure 3.9, then it will be known that this solution is local again. The verification method is able to verify it as well, as it produces zero objective

function value. The final solution *S3* is the minimum solution and is also confirmed by the verification method. It was observed in overall experimentation that, almost one third of the case studies required verification module from 2 to 45 times. This case study concludes that the employed verification module is able to detect the local and is also able to provide an initial condition which further helps in minimizing the solution of scaled minimax. Although, if the objective function value for scaled minimax solution *S1* is compared with the final solution *S3*, a very small improvement (less than 1%) is observed which is practically not significant. The next case study provides an estimate on the improvement in solution achieved with the help of verification module.

(ii). The case study presented here validates that the verification module can be of practical importance in improving the solution of scaled minimax algorithm. The basic parameters for case study design are presented in Table 3.6.

Table 3.6: Design parameters for case study 3

No of points, *n*	99
Initial transformation vector $(t_x(mm), t_y(mm), \theta(radian))$	1, 1, 0.01
Manufacturing error (6σ)	0.001
Scaling constant, *S*	0.5

The transformation parameters for the converged solutions of scaled minimax algorithm and verification module are listed in Table 3.7. Similar to the previous case study, this case also utilizes three initial conditions provided by the verification module. The point to be noted here is that the relative improvement in the objective function value of scaled minimax solution *S3* over *S1* is more than 20%, which quite significantly impacts the minimum zone solution.

Table 3.7: Transformation parameters for scaled minimax method and the verification method for each local solution (Case study-3)

	Scaled minimax method				Verification method			
	Tx	Ty	Theta	Obj Fun	Tx	Ty	Theta	Obj Fun
S1	1.01E-02	-8.57E-03	3.39E-05	3.53E-04	1.01E-02	-8.58E-03	3.36E-05	0
S2	1.02E-02	-9.13E-03	2.13E-05	3.18E-04	1.02E-02	-9.14E-03	2.11E-05	0
S3	1.02E-02	-9.87E-03	5.36E-06	2.79E-04	1.02E-02	-9.87E-03	5.36E-06	3.11E-15

The objective function form of this case was also plotted and analyzed. For this case, *Tx* is kept fixed and objective function is plotted for a varied T_y and *Theta* over the range of solution *S1* to *S3*. Figure 3.10 shows the 3D view of objective function form. The approximate local solutions *S1, S2* and *S3* can be easily located in the graph. Another $y - z$ view of objective function form is presented in the Figure 3.11. This figure again confirms the irregularity of the function near minimum. It can be observed that the function form is same for both the cases. Also, the non smoothness of objective function is of local-local nature, as there are no major peaks and troughs are observed. The irregular nature of this objective function results from the fact that there are many points near optimum which are competing for the minimum zone. It is believed that the relative size variation of locals in different cases depends on the relative distribution of data points; however it is not easy to predict the exact relation.

From both the case studies in this section, it can be concluded that the verification module is effective in determining the local nature of the solution achieved from scaled minimax. And the iterative process of scaled minimax and verification method provides a solution at least equally good as the one will be provided by the zone fitting method alone.
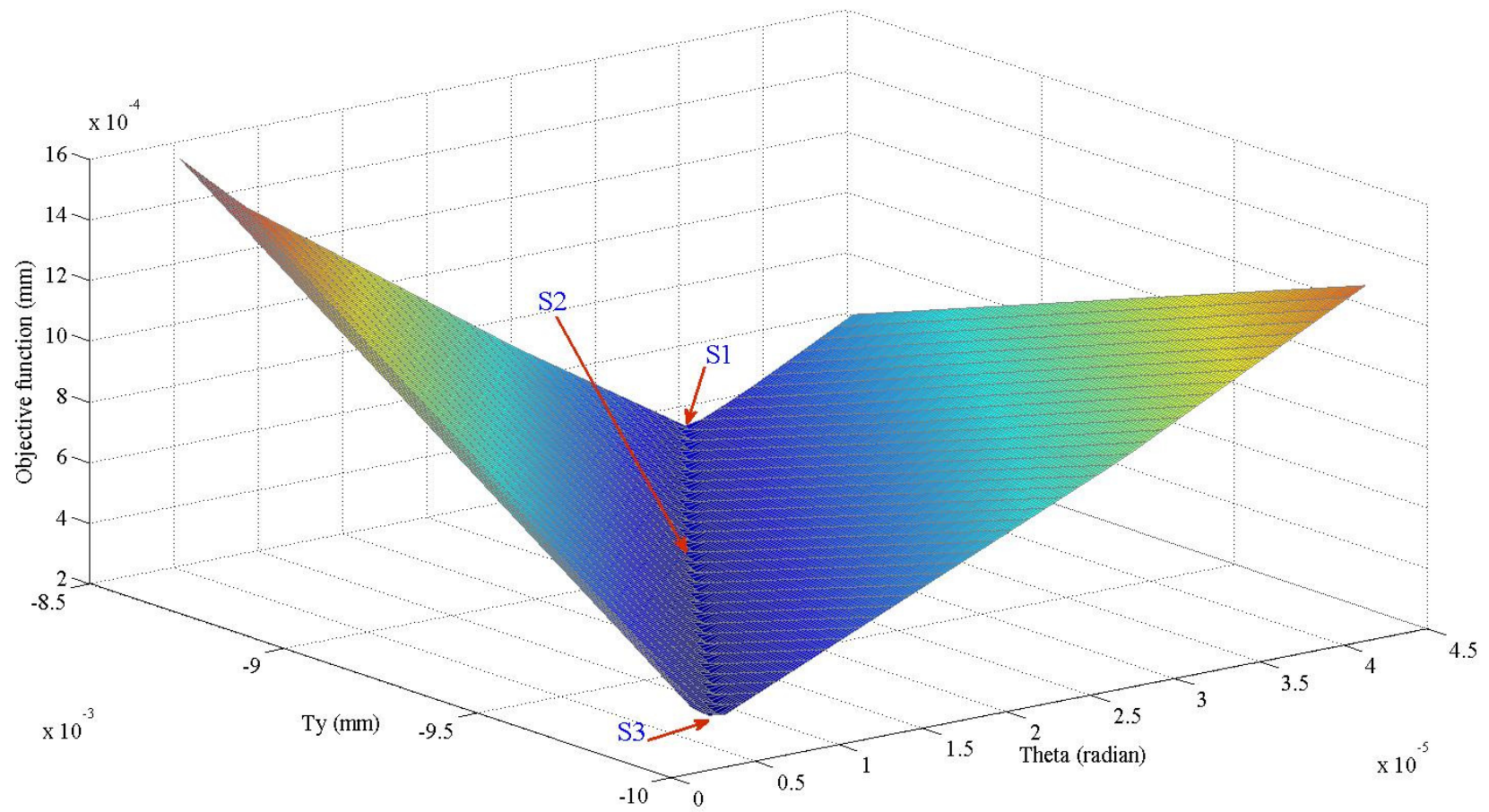
Figure 3.10 : 3D plot objective function form for case study -3. Local minima S1, S2, and S3 are also indicated
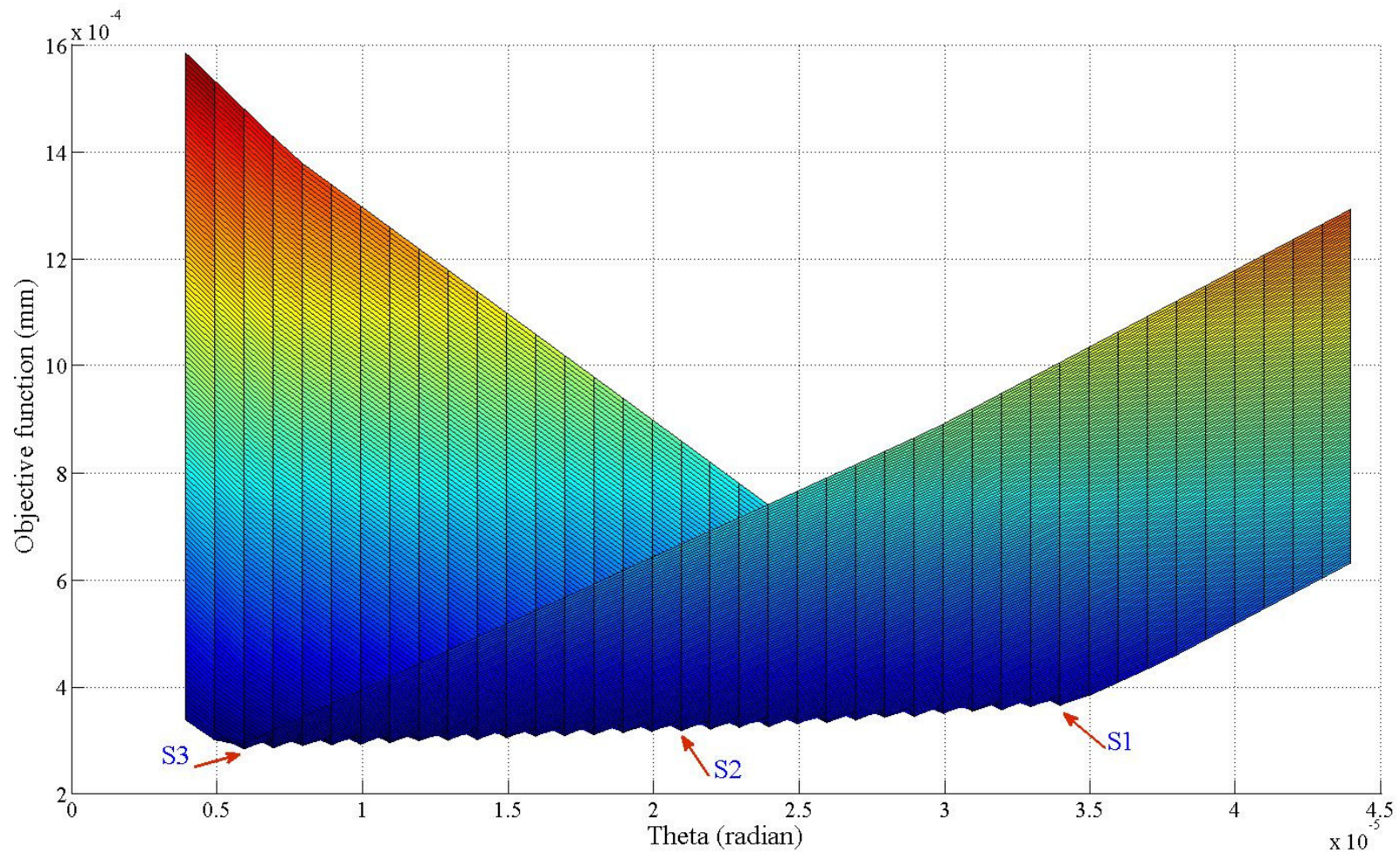
Figure 3.11: y-z perspective of the 3D objective function form plot shown in Figure 3.10. The verification module provides an initial condition which minimizes the scaled minimax solution S1 to S2 and then S2 to S3. The overall improvement in objective function value is ~20%

4 Thickness Control Zone Evaluation

4.1   Introduction

Thickness control zone is a tolerance applied on the airfoil section in order to control the overall shape variation along the pressure and suction sides. The overall shape control of airfoil section is important as it is responsible for the passage created between the two consecutive blades, via which the air passes through. Therefore, it affects the performance of an impeller significantly. As described in Chapter 1, the current literature in the domain of blade parameter evaluation mainly focuses on the evaluation of profile tolerance and the thickness dimension of an airfoil section. However, this is to be noted that profile tolerance and thickness dimensions are not sufficient parameters to control the quality of manufactured airfoil sections. Profile tolerance only controls the form of individual pressure and suction sides. And, thickness dimensions only control the localized leading edge thickness, the trailing edge thickness and the maximum thickness on the airfoil sections. Therefore, it is important to evaluate a parameter which signifies the overall shape variation of the manufacture blade. Hence, there is a need for the development of a method to evaluate thickness control zone.

Thickness control zone is a less known tolerance measure and not explicitly defined in the Dimensioning and Tolerancing standards. However, the basic purpose of thickness control zone tolerance is analogous to the size tolerance. Hence, to further illustrate on the thickness control zone tolerance, an analogy with size tolerance for prismatic components has been described here [13].
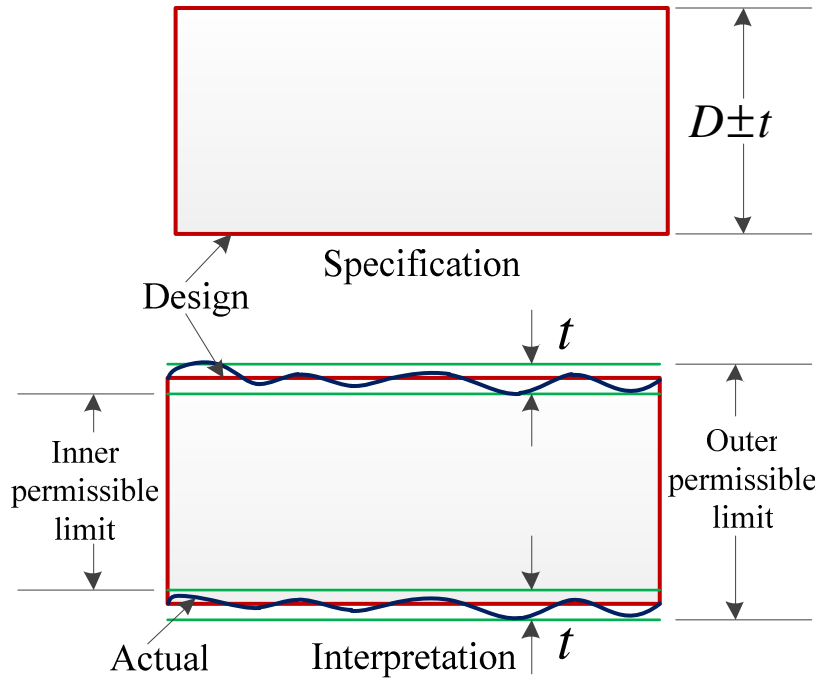
Figure 4.1: Size tolerance for a prismatic component

The tolerance of a size is defined as the difference between the upper and lower limit dimensions of a component. Referring to the Figure 4.1 , the basic size *D* of a prismatic component is allowed to vary between the outer permissible limit of *D+t* and inner permissible limit of dimension *D-t*. Furthermore, it is the tolerance zone of dimension *t* about the design profiles on each side of the component, within which the manufactured profile is allowed to vary. Due to uniform dimension in prismatic components, it is easier to specify the size tolerance for both the sides with respect to a single basic dimension. And also, to inspect the size tolerance; standard gauging methods can be used. However, in case of airfoils, the thickness is continuously varying along the pressure and suction sides. Hence, the thickness control zone is defined in terms of a zone value attached to the nominal. Furthermore, the evaluation of thickness control zone cannot be performed using standard method of gauging. Therefore, a

mathematical model is needed to be developed from the measurement data points to estimate the thickness control zone error.

The subsequent sections in this chapter discuss further details on thickness control zone, followed by the methodology and mathematical formulation to evaluate the thickness control zone tolerance from measurement points. Three case studies are also presented and discussed to validate the implemented algorithm.

4.2   Definition

Thickness control zone is created by simultaneously applying the deviations in a direction normal to the nominal profiles of the pressure and suction sides of an airfoil sections as shown in Figure 4.2. Deviations assigned in the outward direction to the nominal create an outer envelope while the deviations in inward direction create an inner envelope. It is crucial to emphasize here that the outer envelope and inner envelopes are applied simultaneously on the pressure and suction sides. The zone enclosed by these two envelopes is the allowable control zone for the manufactured shape variation.
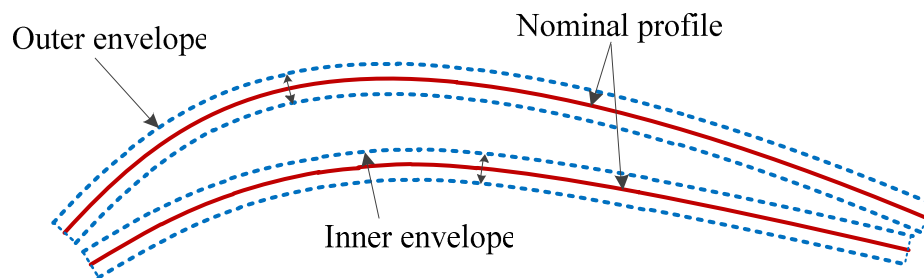
Figure 4.2: Thickness control zone defined by an outer envelope and inner envelope around the nominal suction and pressure side profiles

Furthermore, as discussed in Chapter 3, pressure and suction sides of airfoil section are also assigned with profile tolerances. Therefore, there are multiple tolerances on the airfoil

section, which needs to be satisfied together. This situation is also referred to as the composite tolerancing [13]. The profile tolerance and thickness control zone both are zone type tolerances. Therefore, zone corresponding to one tolerance must be contained inside the other. ASME standard of Dimensioning and Tolerancing, states that in case of composite tolerancing, size tolerance zone contains any other type of geometric tolerances [13]. Therefore, profile tolerance zone will be contained inside the thickness control zone. Moreover, the profile tolerance is related to the form variations of individual sides, while thickness control zone is responsible for the overall shape variations of airfoil section. Therefore, form variations cannot exceed the shape deviations. This discussion becomes important as during thickness control zone evaluation, profile tolerance will act as a constraint, so that both the outer and inner envelopes of the thickness zone are either at the profile zone boundary or exceeding that. The Figure 4.3 shows an overall definition of thickness control zone with the profile tolerance constraints. Therefore, to evaluate the thickness control, a minimum control zone formed the measurement points of pressure and suction side needs to be evaluated, which will be characterized by the maximum outer boundary and minimum outer boundary. Also, these boundaries should contain the profile tolerance zone inside them.
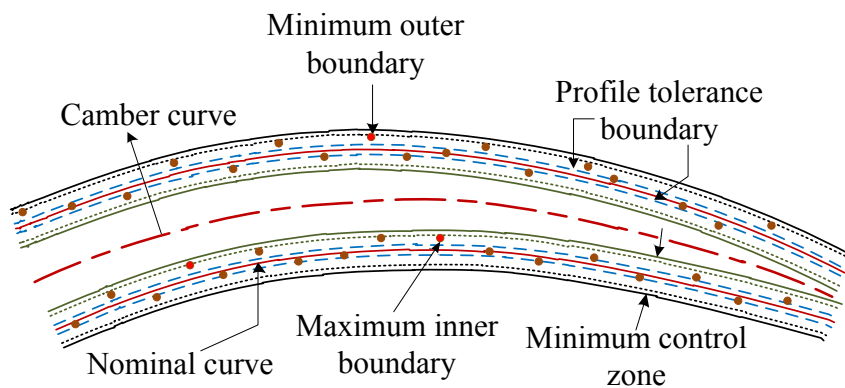
Figure 4.3: Thickness control zone and the profile constraints

4.3 Methodology

For determining the thickness control zone error, the measurement points for pressure and suction sides of an airfoil section are compared with the nominal curves simultaneously. As the design coordinate system (DCS) and the measurement coordinate systems (MCS) are different, a coordinate transformation needs to be determined which can transform measurement points to the design coordinate frame. The measurement points are not exact replica of the points on nominal curves due to the manufacturing errors and the setup errors. Hence, the deviation between measured points and nominal curves should be minimized based an objective function which is consistent with the tolerance under consideration.

The key objective behind thickness control error is the evaluation of a minimum zone about the nominal profiles of pressure and suction sides such that the measurement points for both curves lie inside that zone. The proposed method in this thesis to achieve the stated objective is to shrink the outer boundary and expand the inner boundary formed by measured points, so that the zone encompassed by both boundaries is minimized. The outer and inner boundaries are determined by the maximum-deviation measurement point from the pressure and suction sides in outward and inward directions, respectively. The important point to note here is that for thickness control error evaluation, pressure and suction sides are treated as an integrated geometric element.

Figure 4.4 illustrates the concept of thickness error evaluation. For simplicity, if the pressure and suction sides are represented as semi circles, then outer and inner boundaries will be established as concentric circles. And the control zone will be the difference in radii of these two circles. In order to minimize the control zone, outer boundary will shrink inwardly while inner

boundary will grow outwardly. However, for airfoil sections, such symmetry does not exist and the control zone is established as the sum of normal maximum deviations on outer and inner side.
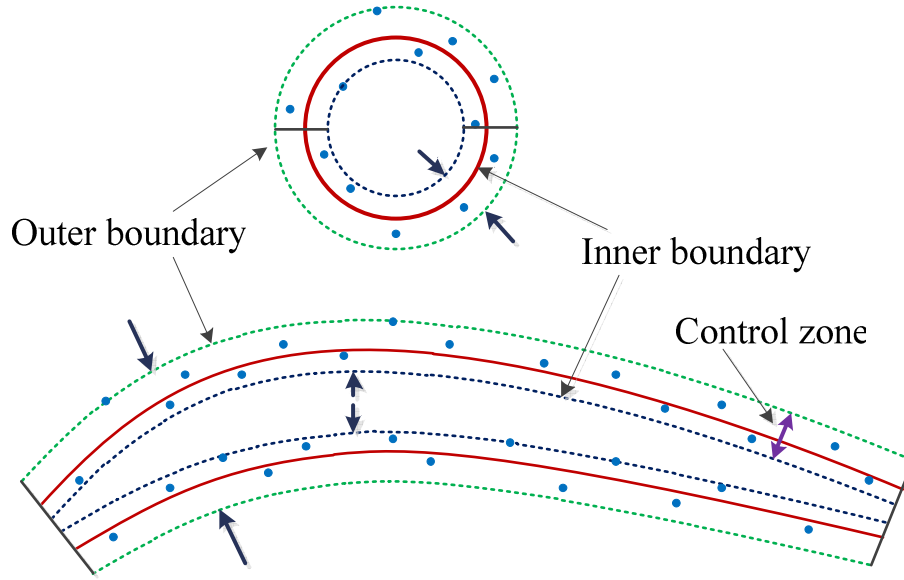
Figure 4.4: Illustration of thickness control zone methodology with an example of semi circle shape pressure and suction sides

4.4 Mathematical formulation

Let the measurement points for pressure and suction sides are represented by Q_i where $i = 1 \ldots q$ and the transformation vector $[t_x, t_y, \theta]$ transforms the points to the design coordinate system. Hence, the newly positioned measurement points Q_i^* can be determined by following equation:

$$Q_i^* = R(\theta) \times (Q_i + T(t_x, t_y)) \qquad (4.1)$$

where, $R(\theta)$ is the rotational matrix and $T(t_x, t_y)$ is the translational vector.

79

From the transformed measurement points, the outer and inner boundaries can be established based on the maximum deviation points. Let the outer deviations are represented by d_outer and inner deviations are represented by d_inner, then the thickness control zone can be formulated as follows:

$$N = \max(d\_outer) + \max(d\_inner) \tag{4.2}$$

The positions of points and their deviations are functions of the coordinate transformation vector. Hence, in order to determine the minimized zone, the formulation is used as an objective function for the search of the transformation parameters. And the search of parameters can be modeled as an optimization problem.

The optimization model is formulated as follows,

$$Obj = \min(N) \tag{4.3}$$

where, thickness zone N is a function of t_x, t_y, θ.

4.5   Detailed procedure

The flow chart in Figure 4.5 shows the important steps to evaluate the thickness control zone error from the measurement data points. As described in Chapter 3, for an initial alignment of the measurement data points and the nominal curve, the transformation matrix is determined using the principal component analysis (PCA) method. The measurement points for the pressure side (PS) and the suction side (SS) are considered together for this initial transformation matrix determination. Thereafter, to determine the deviations of measurement points from nominal, the corresponding points are established on the pressure and suction sides individually. The method

of closest point determination as described in Chapter 3 is used for this algorithm. Subsequently, the location of measurement points with respect to the nominal curve is determined based on the direction of vector product. Location determination method is also similar to the one described in Chapter 3. The remaining important steps for the thickness control zone evaluation are described in detail in this section.
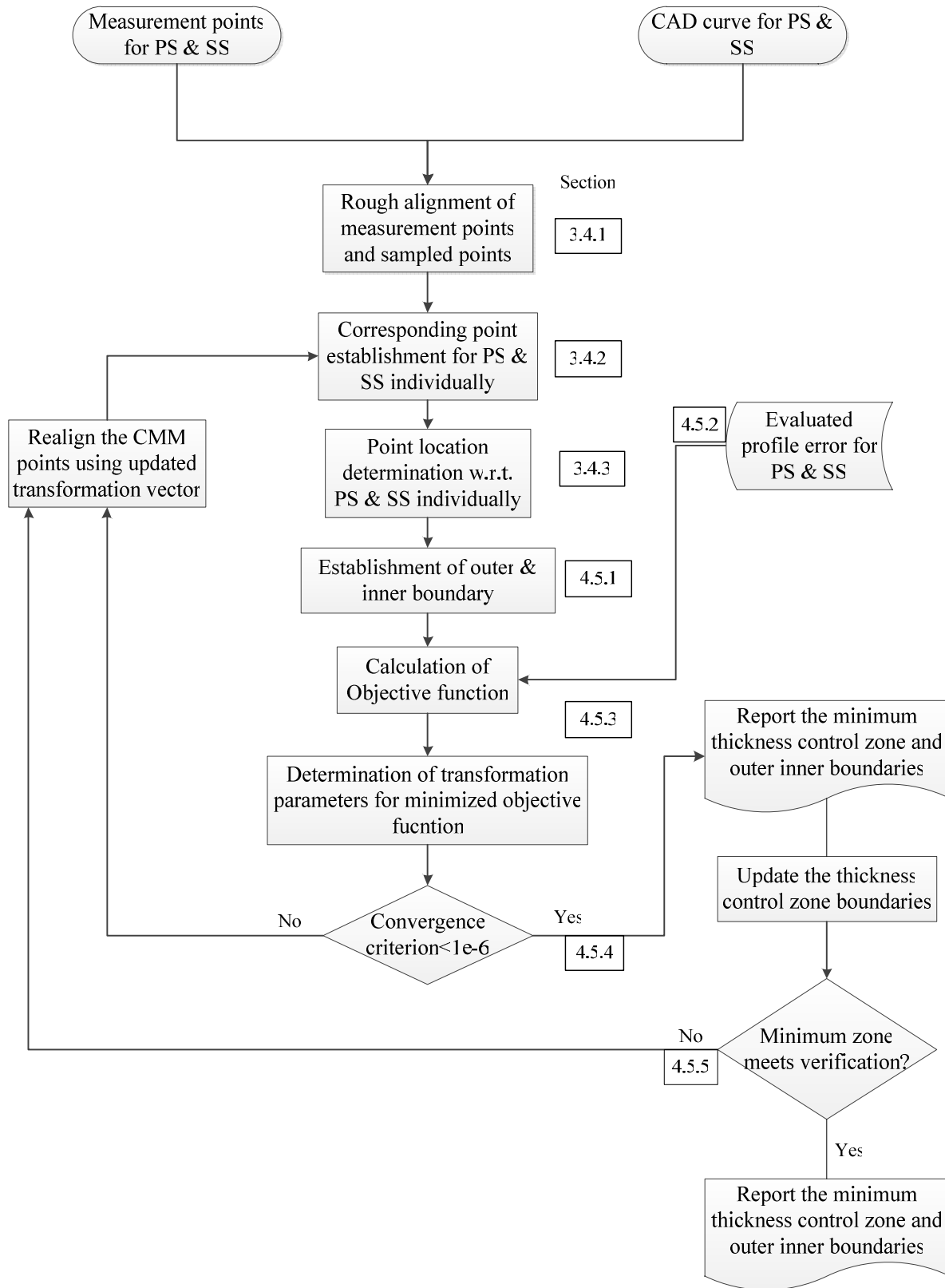
Figure 4.5: Flowchart for thickness control zone evaluation

4.5.1 Outer and inner boundary establishment

After initial alignment, maximum deviations of measured points on each side of the suction and the pressure sides are calculated. Let the maximum deviations on suction sides are represented by d_S_outer, d_S_inner and on pressure side d_P_outer, d_P_inner. The outer-most and inner-most boundaries of thickness zone will be passing through the two maximum deviation points in outward and inward directions respectively and can be calculated as following:

$$\delta\_outer = \max(d_S\_outer, d_P\_outer) \tag{4.4}$$

$$\delta\_inner = \max(d_S\_inner, d_P\_inner) \tag{4.5}$$

4.5.2 Profile error constraint

As described in section 4.2, the profile error zone should be contained in the thickness control zone. Hence, profile error zone will act as a constraint on the established outer and inner thickness control boundaries. The profile error zone for both the pressure and the suction side should lie in the thickness control zone established by the outer and the inner boundaries. As the profile error for pressure and suction sides are evaluated individually, the profile error zones and their respective outer and inner boundaries will not be equal. Hence, if the larger of the profile error boundary on inner and outer sides are contained within the thickness control zone envelope, then it will naturally contain the smaller profile error boundaries. Therefore, based on the evaluated profile errors for pressure and suction sides, constraint boundaries are calculated as following:

$$\zeta_{outer} = \max(E_S\_outer, E_P\_outer) \tag{4.6}$$

$$\zeta_{inner} = \max(E_S \_ inner, E_P \_ inner) \qquad\qquad (4.7)$$

where, ς_{outer} and ς_{inner} are the profile constraints for thickness control zone. $E_S \_ outer$, $E_S \_ inner$ and $E_P \_ outer$, $E_P \_ inner$ are the evaluated outer and inner boundaries of profile tolerance zone on the suction side and pressure sides respectively

To determine whether the profile error constraint lies inside the thickness control zone envelope or not, the Euclidean distance between the corresponding data point on nominal and the measurement data point cannot be used for comparison. Instead, it is the perpendicular distance which should be compared with the profile tolerance constraint boundary. Figure 4.6 illustrates the case, where, during minimization of objective function, the maximum-deviation measurement point lies inside the profile error constraint boundary. The point pair distance δ being maximum deviation will be considered for the thickness boundary establishment. However, if the point pair distance δ is also considered for checking the containment of profile error boundary then it will suggest that the thickness envelope boundary is lying outside of the profile error boundary. Therefore, the normal distance δ' of the maximum-deviation point is always being considered for the checking violation of zone containment.
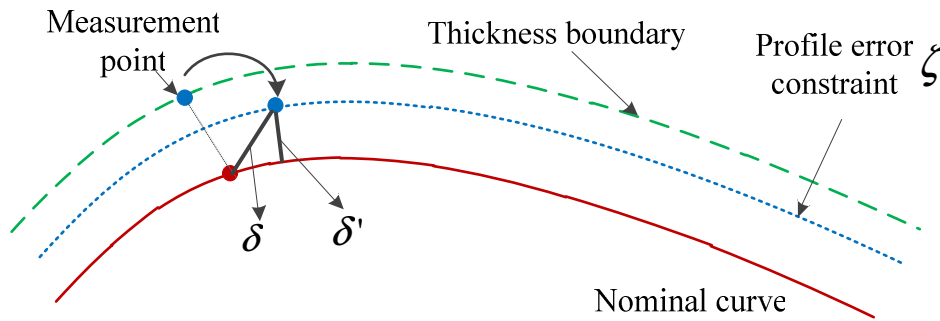
Figure 4.6: Zone containment check using the normal deviation of the maximum-deviation measurement point

4.5.3   Objective function evaluation

The value of objective function is evaluated as the sum of maximum deviations on the inner side and the outer side. If the maximum-deviation point corresponding to the outer envelope or the inner envelope lies inside the profile error boundary, then it violates the zone containment condition. Hence, the formulation needs to be modified such that optimization can force the maximum-deviation points to lie outside of the profile constraint boundaries. This is done by assigning a penalty function, so that objective function value becomes very high when maximum-deviation point lies inside and therefore, optimization will try to search for a transformation which can bring the maximum-deviation points outside the constraint boundary and thus reduce the objective function value.

Penalty function can be designed in various ways. The idea is to heavily penalize the distance by which maximum-deviation point is lying inside the constraint boundary. In the implemented algorithm, a linear penalty function is designed such that it imposes maximum penalty to the point when maximum-deviation point lies on the nominal and minimum penalty when maximum-deviation points lies on the constraint boundary. The penalty function is represented by following equation,

$$PF = (\zeta - \delta^{'}) * K \tag{4.8}$$

where, K is a very large number. In the implemented algorithm, the value of K has been considered as 1e07. $\delta^{'}$ is the normal distance of the maximum-deviation measurement point from the nominal. Penalty function is evaluated individually for the outward and the inward side of the nominal.

The outer envelope N_{outer} of thickness control zone can be evaluated as follows:

$$N_{outer} = \begin{array}{ll} \delta_{outer} & if \quad \delta_{outer}' > \zeta_{outer} \\ \delta_{outer} + (\zeta_{outer} - \delta_{outer}') \times K & if \quad \delta_{outer}' < \zeta_{outer} \end{array} \qquad (4.9)$$

The inner envelope N_{inner} of thickness control zone can be evaluated as follows:

$$N_{inner} = \begin{array}{ll} \delta_{inner} & if \quad \delta_{inner}' > \zeta_{inner} \\ \delta_{inner} + (\zeta_{inner} - \delta_{inner}') \times K & if \quad \delta_{inner}' < \zeta_{inner} \end{array} \qquad (4.10)$$

The control zone N, which acts as objective function can be calculated as follows:

$$N = N_{outer} + N_{inner} \qquad (4.11)$$

To minimize the thickness control zone, the parameters of coordinate transformation are searched in the domain space. The formulation of objective function is a non linear unconstrained problem. Therefore, the problem needs to be solved iteratively. Also, the first derivative of objective function is not continuous in nature. Therefore, a direct search technique needs to be employed to evaluate the parameters. Similar to profile tolerance evaluation, downhill simplex search technique is being used here for the optimization. *Fminsearch* routine of MATLAB is utilized for minimization.

4.5.4   Iteration and convergence

The optimization routine determines the transformation parameters such that for established corresponding point sets, the thickness control zone is minimized. However, the initial correspondence is not necessarily the right correspondence. Therefore, for the next iteration, corresponding points are again established based on the closest point concept. This iteration between corresponding point establishment and the determination of transformation parameters for a minimum zone is carried out till a convergence criterion is met. The

convergence criterion has been set here as the relative change in the objective function. Therefore, when the convergence criterion becomes less than a specified tolerance, the iteration stops and algorithm returns the minimized zone and corresponding transformation parameters.

4.5.5 Verification of the evaluated zone

The direct search methods employed for the optimization are known to give local solutions. In the current situation, problem being non linear in nature, there is a high probability for the achieved solution being a local minima. Therefore, there is a scope for verification of the achieved solution from the control zone evaluation algorithm.

The idea of verification is very similar to that of the profile tolerance zone as described in Chapter 3. The verification is performed using zone fitting method [21]. The evaluated control zone boundaries are shrunk by a small amount and then using the zone fitting method, a transformation is searched which can place points within the updated boundaries. Zone fitting method produces objective function as zero if all the points are contained within the boundaries otherwise it is a non zero value. A zero objective function shows that a further minimum zone is available and the set of transformation parameters corresponding to zero objective function, act as an initial condition for the control zone evaluation algorithm for further minimization. However, the original zone fitting formulation alone will not be suitable to the thickness control zone case, as the thickness control zone additionally demands to meet the profile tolerance constraint. Hence, a modification is required in the formulation, so that transformation is sought only in the available space between the updated boundaries and the profile constraint boundaries.

Let the evaluated boundaries from the thickness control zone algorithm be N_{outer} and N_{inner}. For verification, the boundaries are shrunk by a small pre-specified resolution. The

87

resolution is considered as 0.01%. Hence, the updated boundaries of control zone can be determined as follows:

$$N_{outer}{}' = N_{outer} \times (1 - resolution) \qquad (4.12)$$

$$N_{inner}{}' = N_{inner} \times (1 - resolution) \qquad (4.13)$$

The objective function of the zone fitting is modified by adding two additional terms. The modified objective function is defined as follows:

$$Obj = Obj_{zone\_fitting} + PF_{outer} + PF_{inner} \qquad (4.14)$$

The first term in Equation (4.14) is the truncated least square function. For pressure and suction sides, the truncated least square function is evaluated individually. Equation (4.15) presents the objective function formulation for zone fitting. This formulation is described here for suction side only. Same formulation will be applicable to the pressure side as well and sum of objective function for both sides will form the first term in Equation (4.14).

$$Obj_{zone\_fittingS} = \sum_{i=1}^{i=n} r_i^2 \qquad (4.15)$$

where,

$$r_i = \begin{cases} (dist(m,S) - N_{outer}{}')^2 & if \quad N_{outer}{}' \le dist(m,S) \\ 0 & if \ N_{inner}{}' \le dist(m,S) \le N_{outer}{}' \\ (dist(m,S) - N_{inner}{}')^2 & if \quad dist(m,S) \le N_{inner}{}' \end{cases} \qquad (4.16)$$

here, $dist(m,S)$ represents the deviation of the measurement point from the nominal. Updated thickness control zone boundaries are represented by $N_{outer}{}'$ and $N_{inner}{}'$. The mathematical

formulation in Equation (4.16) indicates that when all the measurement points are inside the updated thickness control zone boundaries, then the zone fitting objective function value will become zero.

The second term PF_{outer} in Equation (4.14) represents the penalty function due to the outer profile constraint boundary. During verification of new updated thickness control zone boundaries, the measurement points are forced to lie inside the updated thickness control zone boundaries. However, the points need to be transformed in such a way that the profile constraint is not violated. Therefore, a penalty function has been introduced in the verification method. The mathematical formulation of this function is given as follows:

$$PF_{outer} = \begin{array}{ll} 0 & if \quad \delta_{outer}' > \zeta_{outer} \\ \delta_{outer} + (\zeta_{outer} - \delta_{outer}') \times K & if \quad \delta_{outer}' < \zeta_{outer} \end{array} \tag{4.17}$$

The third term PF_{inner} in Equation (4.14) represents the penalty function due to the inner profile constraint boundary. PF_{inner} is also evaluated similar to PF_{outer}. The mathematical formulation of this penalty function is given as follows:

$$PF_{inner} = \begin{array}{ll} 0 & if \quad \delta_{inner}' > \zeta_{inner} \\ \delta_{inner} + (\zeta_{inner} - \delta_{inner}') \times K & if \quad \delta_{inner}' < \zeta_{inner} \end{array} \tag{4.18}$$

Thus, the overall thickness control zone algorithm has two components: thickness control zone evaluation and the zone verification. And these two steps are iterated until an updated thickness control zone boundaries are achieved which are confirmed by the modified zone verification method.

4.6 Case studies

25 case studies are tested with the implemented algorithm with the intent to test the multiple aspects of developed method. Three representative case studies are presented here for discussion purpose. The first case study checks if the implemented algorithm converges to an expected solution. Second case study demonstrates the importance and requirement of a thickness control zone specification on an airfoil section. And the third case study examines the impact of profile constraint boundaries on the evaluated minimum thickness control zone.

4.6.1 Case study design

To simulate the data points for case studies, first pressure and the suction sides are created as cubic curves. Thereafter, to simulate the measurement points, manufacturing error is generated corresponding to a normal distribution and assigned on the sampled points on the pressure and suction curves. Noise is assigned in a perpendicular direction to the nominal curve. An initial transformation is also applied to these generated points to simulate a situation of inconsistency between the design coordinate system and measurement coordinate system. The Figure 4.7 shows the design of a typical case study for thickness control zone evaluation. The figure shows theoretical curves for pressure and suction sides, and also simulated measurement points corresponding to each curve. All the case studies presented here are created in similar way with some customization to each case study, which will be discussed in respective section.

For thickness control zone evaluation, it is necessary to evaluate the profile tolerance of pressure and suction sides first, as the profile constraint boundary is deduced from the evaluated profile tolerance zones. Thereafter, the same simulated data set is applied to the thickness control zone evaluation algorithm.
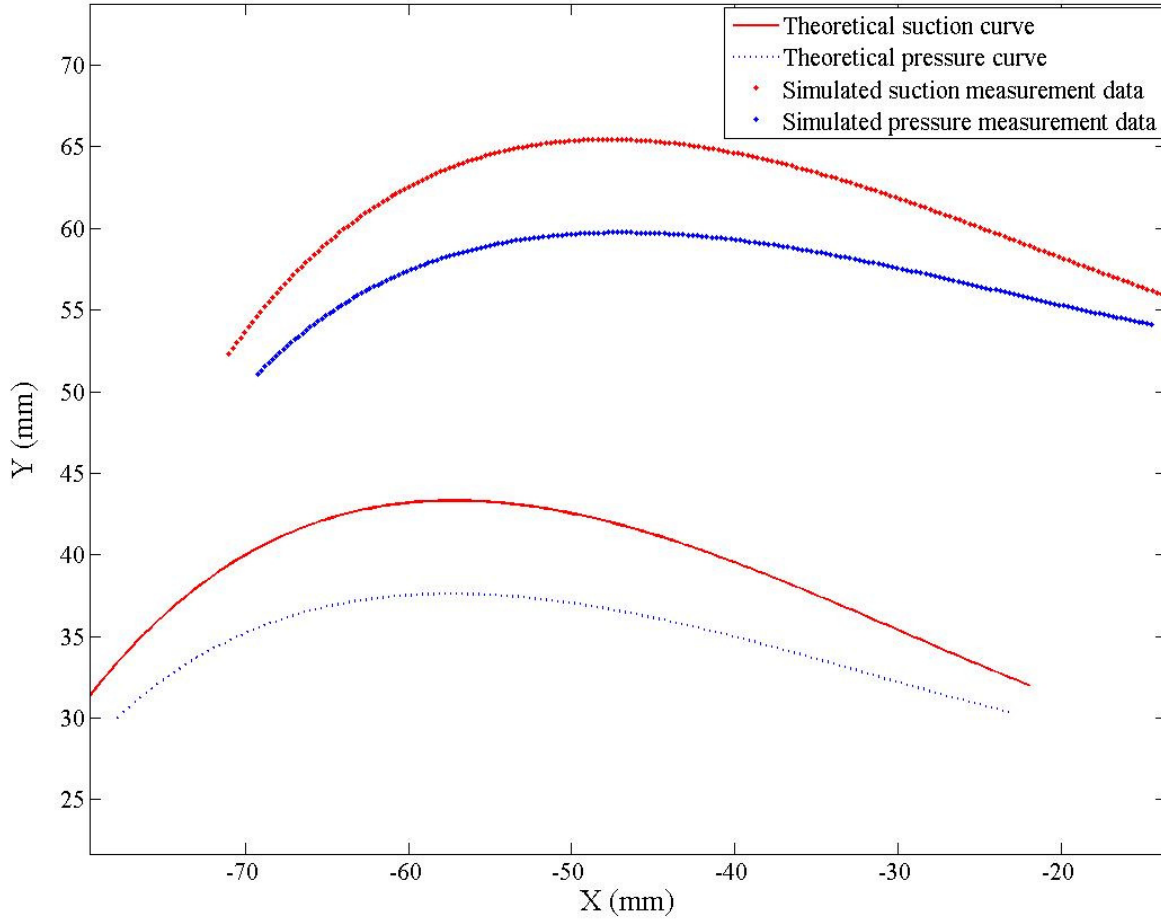
Figure 4.7: Typical case study design for thickness control zone evaluation

For validation of the converged solution from the thickness control zone, there is no theoretical zone available to compare with. However, the initial zone created by assigning the measurement uncertainty is one of the solutions for the evaluated zone. Hence, it is expected that the algorithm should converge to an equal or smaller zone.

4.6.2 Case study 1: convergence to the expected solution

This case study has been designed to check if the implemented algorithm of thickness control zone converges to an expected solution. Table 4.1 shows the basic parameters for the case design. The important point to note here is that scaling constants *S1* and *S2* for profile

tolerance evaluation of the pressure and the suction sides are chosen as the ratio of initial outer and inner boundaries. This careful selection helps in attaining the initial condition as a valid solution for the thickness control zone. The valid solution is the one in which the evaluated profile error boundaries are contained inside the initial boundaries of simulated data points. Valid solution ensures that the profile constraint is not violated and therefore, an initial thickness control zone can be deduced from the simulated data points.

Table 4.1: Design parameters for case study 1

No. of points on each curve	199
Initial transformation vector $(t_x(mm), t_y(mm), \theta(radian))$	10,12,1E-05
Manufacturing error on SS	7E-04
Manufacturing error on PS	5E-04
Resolution	0.01%
S1	1.1661
S2	1.1015

For evaluating thickness control zone, first, profile tolerance evaluation for the pressure and suction side is performed individually using the algorithm defined in Chapter 3. Table 4.2 lists the outer and inner limits of the initial zone for suction side (SS), pressure side (PS) and their corresponding evaluated profile tolerance zone values. Table shows that the evaluated outer and inner boundaries of suction and pressure side are within their respective initial outer and inner boundaries. Therefore, a valid initial thickness control zone can be deduced here.

Table 4.2: Profile tolerance results for pressure and suction sides for case 1. Zone value is the sum of outer and inner boundary. All values in mm

	Initial zone SS	Evaluated zone SS (E_S)	Initial zone PS	Evaluated zone PS (E_P)	Initial thickness control zone
Outer	3.61E-04[#]	3.45E-04[*]	2.19E-04	2.08E-04	3.61E-04

boundary					
Inner boundary	3.09E-04[#]	2.96E-04[*]	2.41E-04	2.29E-04	3.09E-04
Zone value	6.70E-04	6.40E-04	4.60E-04	4.38E-04	6.70E-04

Note: * represents the values corresponding to the profile constraint boundaries. # represents maximum of the outer and inner boundaries from initial zone of suction and pressure side, which makes the initial thickness control zone.

The thickness control zone is defined as the sum of maximum deviation on the outer and inner side. Table 4.2 shows, that the initial outer boundary for suction side is larger than the initial outer boundary on pressure side. Therefore, the larger value is chosen as the outer boundary of thickness control zone. Similarly, for inner side, maximum of the initial deviations on pressure and suction sides are chosen as initial inner boundary of thickness control zone.

Table 4.3: Evaluated thickness control zone error. All values in mm

	N_{outer}	N_{inner}	Thickness control zone
Initial	3.61E-04	3.09E-04	6.70E-04
Evaluated	3.45E-04	2.96E-04	6.41E-04

The data set is further evaluated for thickness control zone evaluation. Table 4.3 lists the outer and inner boundaries of evaluated thickness control zone. This can be observed from the Table 4.3, that the evaluated thickness control zone is smaller than the initial thickness control zone. As the converged solution is smaller than the initial solution therefore it can be concluded that the implemented algorithm is converging to the expected solution.

4.6.3   Case study 2: demonstration of utility of thickness control zone

This case study demonstrates a situation, which shows the significance of the thickness control zone tolerance for airfoil geometry. Profile tolerance alone is not a sufficient tolerance for controlling the form and shape of the airfoil section. While designing the simulated data for this case study, purposely, points of pressure and suction sides were not assigned any uncertainty. This suggests that the form of the pressure and the suction side is perfect in nature and therefore, there is no profile error associated with them. Furthermore, sampled points on the suction curve were offset in positive y-direction and sampled points on pressure curve were offset in negative y-direction. The offset data points created a shape which is significantly deviated (thicker) from the theoretical shape. The offset points were also transformed using an initial transformation. It is expected that the deviation in the generated shape should be captured during the thickness control zone evaluation. Table 4.4 lists the basic parameters for the design of case study.

Table 4.4: Design parameters for case study 2

No. of points on each curve	199
Initial transformation vector $(t_x(mm), t_y(mm), \theta(radian))$	15,10,1E-04
Manufacturing error on SS	0
Manufacturing error on PS	0
S1	1
S2	1
Outward offset vector SS	0,0.005,0
Outward offset vector PS	0,0.005,0

The simulated data set was evaluated for the profile tolerance for pressure and suction sides individually. The evaluated profile tolerance was reported as zero for both pressure and suction sides. This result signifies the perfect form of pressure and suction sides individually. However, this result is not able to capture the initial significant deviation assigned in the

94

simulated data. Therefore, another tolerance measure of thickness control zone is required. This measure accounted the measurement data for pressure and suction side together and thus it was expected to capture the overall deviation in the generated shape.

Table 4.5: Evaluated outer and inner maximum deviations for pressure and suction side for case study-2

	d_S_outer	d_S_inner	d_P_outer	d_P_inner	Thickness zone
Initial	5.00E-03	0	5.00E-03	0	5.00E-03
Evaluated	5.00E-03	0	5.00E-03	0	5.00E-03

The simulated data was further tested with the thickness control zone algorithm. Table 4.5 reports the evaluated outer and inner maximum-deviations for the pressure and suction sides. The evaluated maximum outer deviations are same as original offset assigned on the theoretical profile. Therefore, it can be concluded that the thickness control zone is able to detect the overall deviations in the shape of airfoil section which otherwise cannot be predicted by the profile tolerance zone. Hence, for quality inspection both measures of profile tolerance and thickness control zone are required.

4.6.4 Case study 3: impact of profile constraint

This case study studies the impact of profile constraint employed in the thickness control zone evaluation. Profile error zone acts as a refinement of the pressure and suction surface and therefore, it cannot exceed the thickness control zone. Hence, it is employed as a constraint in the evaluation of thickness control zone. To examine the effect of profile tolerance constraint on the evaluated thickness control zone, case studies are evaluated with and without profile error constraints. Two case studies are presented in this category.

(i) No impact of profile constraints on the evaluated thickness control zone

The first case study presented here represents the cases, in which the profile tolerance constraint did not impact the solution of thickness control zone. Hence, it is expected that the zone evaluated with and without profile constraints should result same. Table 4.6 shows the basic parameters of this case study.

Table 4.6: Design parameters for case study 3(i)

No. of points on each curve	101
Initial transformation vector $(t_x(mm), t_y(mm), \theta(radian))$	15,10,0.0001
Manufacturing error on SS	8e-04
Manufacturing error on PS	8e-04
Resolution	0.01%
S1	1
S2	1

The data set is first evaluated for the profile error evaluation for pressure and suction sides individually. Table 4.7 shows the results of profile tolerance evaluation. The scaling constants signify that the current case is bilateral symmetric type. Therefore, the evaluated zone boundaries for suction and pressure side are symmetric in nature. Furthermore, the evaluated outer and inner boundaries of pressure side are larger than the evaluated outer and inner boundaries of suction side. Therefore, the evaluated pressure side boundaries will act as the profile constraint for thickness control zone evaluation. Also, it should be observed that the profile constraint boundaries are smaller than the initial outer and inner boundaries of thickness control zone. Hence, the initial control zone can be treated as a valid solution for the comparison with the evaluated zone.

Table 4.7: Results of profile tolerance evaluation for pressure and suction sides. All values are in mm

	Initial zone SS	Evaluated zone SS (E_S)	Initial zone PS	Evaluated zone PS (E_P)	Initial thickness zone
Outer boundary	3.10E-04	3.13E-04	3.23E-04[#]	3.15E-04[*]	3.23E-04
Inner boundary	3.23E-04[#]	3.13E-04	3.10E-04	3.15E-04[*]	3.23E-04
Zone value	6.33E-04	6.26E-04	6.33E-04	6.26E-04	6.46E-04

Note: * represents the values corresponding to the profile constraint boundaries. # represents maximum of the outer and inner boundaries from initial zone of suction and pressure side, which makes the initial thickness control zone.

Table 4.8: Results of thickness control zone for case-3(i) with profile constraints and w/o profile constraints

	N_{outer}	N_{inner}	Thickness control zone ($N_{outer} + N_{inner}$)
Without profile constraints	3.16E-04	3.16E-04	6.32E-04
With constraints	3.16E-04	3.16E-04	6.32E-04

Further, this data set is tested with the thickness control zone algorithm in two situations. First situation considers the established profile constraint during evaluation of thickness control zone and the second situation does not. The results for both situations are listed in the Table 4.8. It can be observed from the table that the evaluated thickness control zone is equal for both situations. Also, it is important to note that the evaluated zone lies outside of the profile tolerance constraint even for the case without profile constraints consideration. This signifies that the profile tolerance constraints didn't play any role during the thickness control zone evaluation. It is believed that when the minimum thickness control zone occurs outside of the profile constraint boundaries, then these constraints do not impact the minimum zone solution. It can be concluded from this case study that though profile constraint boundaries are required during the evaluation

of thickness control zone, it is not necessary that in all the case studies, constraint is being utilized.

(ii) Impact of profile constraints on the evaluated thickness control zone

The second category of cases is where profile error constraint impacts the solution of thickness control zone evaluation. The Table 4.9 shows the basic parameters for the design of case study.

Table 4.9: Design parameters for case study 3(ii)

No. of points on each curve	199
Initial transformation vector $(t_x(mm), t_y(mm), \theta(radian))$	10,10,0.0002
Manufacturing error on SS	6e-4
Manufacturing error on PS	6e-4
S1	1
S2	1

The data set is first evaluated for the profile tolerance zone for pressure and suction sides individually. Table 4.10 suggests that the evaluated profile tolerance zone is inside the initial zone boundaries; therefore, an initial thickness control zone can be deduced. The evaluated inner and outer profile boundaries of suction side are greater than the pressure side; therefore, they will act as the profile constraint during thickness control zone evaluation. Furthermore, in this case too, a valid initial zone can be deduced. Thereafter, simulated data set is tested on thickness control zone with and without profile constraints. Table 4.11 presents the results of thickness control zone for both situations. It can be observed in the Table 4.11 that the solution without considering profile constraint shows that the inner boundary of thickness control zone is smaller than the profile constraint inner boundary. This situation violates the basic premise that form

error should not exceed the thickness control zone. While, the data set is evaluated with constraints, it is evident that both outer and inner boundaries of thickness control zone are lying outside of the profile constraint, which is desirable. Hence, it can be concluded that the employed penalty function for profile constraint is able to meet the specified requirement of containing profile tolerance zone inside the thickness control zone.

Table 4.10: Results: Profile tolerance zone for pressure and suction side

	Initial zone SS	Evaluated zone SS (E_S)	Initial zone PS	Evaluated zone PS (E_P)	Initial thickness zone
Outer	3.58E-04[#]	3.18E-04[*]	3.03E-04	2.58E-04	3.58E-04
Inner	2.94E-04[#]	3.18E-04[*]	2.42E-04	2.58E-04	2.94E-04
Zone value	6.52E-04	6.36E-04	5.45E-04	5.15E-04	6.52E-04

Note: * represents the values corresponding to the profile constraint boundaries. # represents maximum of the outer and inner boundaries from initial zone of suction and pressure side, which makes the initial thickness control zone.

Table 4.11: Results of thickness control zone for case-3(ii) with profile constraints and w/o profile constraints

	N_{outer}	N_{inner}	Thickness control zone ($N_{outer} + N_{inner}$)
Without profile constraints	3.27E-04	3.08E-04	6.35E-04
With constraints	3.23E-04	3.13E-04	6.41E-04

In all the performed case studies, the converged thickness control zone solution was validated by the verification module. The verification module confirmed the first converged solution of thickness control zone and there was no iteration observed between the verification module and thickness control zone algorithm. It is believed that for all the performed case

studies, the first converged solution did not get stuck in the local (it was a minimum solution) and therefore no iteration between thickness control zone algorithm and verification module was reported. It is reasoned that if profile constraint would not have been there, the minimum solution boundaries would have been lesser than the profile constraint boundaries (atleast at one side).Because of the profile constraints, the minimum solution is now occurring outside of the profile constraint boundaries, which is easily detectable for the search algorithm. The verification module will become important for those cases where the profile constraint does not impact the solution of thickness control zone (like case 3(i)) and thus the minimum zone naturally occurs outside of the constraint boundaries. In these situations, the obtained solution will have a higher probability of being a local solution and verification module would be helpful to minimize it further.

5 Conclusion

5.1 Research contribution

This dissertation has presented algorithms for evaluation of geometric errors associated with the pressure and suction sides of an airfoil section. The research work has introduced a novel scheme of scaled minimax to evaluate all three types of profile tolerances: bilateral symmetric, bilateral asymmetric, and unilateral. The thesis also presented a method for evaluation of thickness control zone, a relatively less known tolerance measure of airfoil sections. Furthermore, this work also attempted to utilize the measurement uncertainty information during the reconstruction of pressure and suction side curves. All three contributions are summarized below.

Profile tolerance controls the form of pressure and suction sides of airfoil sections. The basic formulation of presented scaled minimax algorithm is built on the minimax fitting method, which facilitated the use of a scaling constant. The scaling constant can regulate the relative boundary positions of evaluated zone and therefore it enabled the evaluation of all types of profile tolerances. The case studies demonstrated that existing fitting algorithms may experience inconsistency in tolerance zone conformance verification or may fail in case of unilateral tolerances. However, the proposed method of scaled minimax is consistent for all types of tolerance zone conformance. Furthermore, the method has been tested for nonlinear parametric curves of pressure and suction sides. Therefore, it is believed that the method can be extended easily to the profile tolerance evaluation of simple geometries. The minimax formulation is known to have irregularities near the optimum which was also verified from the plot of objective

function presented in a case study. To overcome local minimum nature of objective function, a verification module was proposed. Numerous case studies showed that the incorporation of verification module was successful in overcoming the local minimum of the minimax formulation. A maximum of 20% improvement in objective function value was observed due to the employed verification module. The algorithm of verification module is adopted from the zone fitting method. It is important to state that even though the formulation of proposed algorithm is minimax in nature, it still provides equally good solution as the zone fitting method, because of the employed verification module.

The secondary focus of this thesis was the development of a method for evaluation of thickness control zone. The thickness control zone is a critical parameter which controls the overall shape deviation of an airfoil section between the pressure and the suction sides. The proposed method considers the measurement points of pressure and suction side together to evaluate the thickness control zone. The method establishes an outer and an inner boundary. Thereafter it tries to move them together so that the zone encompassed is minimized. The presented case studies also confirmed the convergence to an expected solution. Furthermore, to accommodate the composite tolerancing situation because of the profile tolerance, a penalty function was used to modify the method. The case studies demonstrated the containment of profile tolerance inside the thickness control zone. Though the thickness control zone presented here is developed and tested only for the airfoil sections. This formulation is expected to be applicable to simple prismatic geometries too.

Lastly, this thesis also considered the measurement uncertainty information associated with measurement results. Profiles of pressure and suction sides were reconstructed within a given measurement uncertainty. Furthermore, a numerical method for camber curve was also

presented which is instrumental in determining the thickness dimensions associated with the airfoil sections. The reconstructed profiles of pressure and suction side can be further sampled to generate the data points, which further acts as an input to the geometric error evaluation algorithms.

5.2 Limitation and future work

The proposed method of scaled minimax is suitable for all possible types of profile tolerance evaluations. However, the scaled minimax formulation depends on the ratio of specified tolerance boundaries. Therefore, it is not suitable for situations where multiple combined features with different tolerance zones need to be evaluated simultaneously. Also, in the dissertation measurement uncertainty is assumed to be given for all the calculations. However, the measurement uncertainty value is not readily available and needs to be calculated from the various factors affecting the coordinate measurement results.

Furthermore, this thesis only covers the tolerance evaluation associated with the pressure and suction sides of individual airfoil sections. Evaluation of leading and trailing edge is the next step to completely inspect a single airfoil section. Furthermore, complete blade inspection, requires orientation tolerance estimation as well. Orientation tolerances determine the relative positioning of multiple airfoil sections.

In the current work, measurement data from touch trigger probe is being considered for evaluation. The work can be extended to the evaluation from the measurement data points acquired via laser scan CMM. However, the sectional information is missing in the inspection data acquired via laser scanning CMM, as laser scans across the complete blade surface.

Therefore, preprocessing on the inspection data is required to derive the sectional information, which can act as an input to the algorithms developed in this thesis.

Bibliography

[1]   Chase, K.W., Greenwood, W.H., Loosli, B.G., and Hauglund, L.F., 1990, "Least Cost Tolerance Allocation for Mechanical Assemblies with Automated Process Selection," Manufacturing Review, **3**(1), pp. 49-59.

[2]   Gao, J., Chase, K. W., and Magleby, S. P., 1998, "Generalized 3-D Tolerance Analysis of Mechanical Assemblies with Small Kinematic Adjustments," IIE Transactions, **30**(4), pp. 367-377.

[3]   Savio, E., Chiffre, L. D., and Schmitt, R., 2007, "Metrology of Freeform Shaped Parts," CIRP Annals - Manufacturing Technology, **56**(2), pp. 810-835.

[4]   Yadong, L., and Peihua, G., 2004, "Free-form surface inspection techniques state of the art review," Computer-Aided Design, **36**(13), pp. 1395-1417.

[5]   Bell, S.A., 2001, *A beginner's guide to uncertainty of measurement*, National Physical Laboratory, United Kingdom.

[6]   Hsu, T. H., Lai, J.Y., and Ueng, W.D., 2006, "On the development of airfoil section inspection and analysis technique." International Journal of Advanced Manufacturing Technology, **30**, pp. 129–140.

[7]   Pahk, H.J., and Ahn, W.J., 1996, "Precision inspection system for aircraft parts having very thin features based on CAD/CAI integration," International Journal of Advanced Manufacturing Technology, **12**, pp. 442–449.

[8]   Chen, L., Li, B., Jiang, Z., Ding, J., and Zhang, F., 2010, "Parameter extraction of featured section in turbine blade inspection," IEEE International Conference on Automation and Logistics, pp. 501-505.

[9]   Jinkerson, R.A., Abrams, S.L., Bardis, L. C., Chryssostomidis, Clement, A., Patrikaiskis , N.M., and Wolter, F.E., 1993, "Inspection and feature extraction of marine propellers," Journal of Ship Production, **9**(2), pp. 88–106.

[10]   Weckenmann, A., Knauer, M., Killmaier, T., 2001, "Uncertainty of coordinate measurements on sheet-metal parts in the automotive industry," Journal of Materials Processing Technology, 115, pp. 9-13.

[11]   Cox, M.G., 1971, "Curve fitting with piecewise polynomials," Institute of Journal of Mathematics and its Applications, 8, pp. 36-52.

[12] Hoschek, J., and Lasser, D., 1993, *Fundamentals of Computer Aided Geometric Design*, A.K. Peters, and Massachusetts.

[13] ASME, 1994, *Dimensioning and Tolerancing*, ANSI Y14.5M – 1994, American Society of Mechanical Engineers, New York, NY.

[14] ASME, 1994, *Mathematical Definition of Dimensioning and Tolerancing Principles*, ANSI Y14.5M – 1994, American Society of Mechanical Engineers, New York, NY.

[15] Feng, S. C., and Hopp, T. H., 1991, "A Review of Current Geometric Tolerancing Theories and Inspection Data Analysis Algorithms," International Journal of Production Research, **40**(11), pp. 24-25.

[16] Menq, C. H., Yao, H. T., and Lai, G. Y., 1992, "Automated precision measurement of surface profile in CAD-directed inspection," IEEE transactions on Robotics and Automation, **8** (2), pp. 268-278.

[17] Murthy, T.S.R., and Abdin, S.Z., 1980, "Minimum zone evaluation of surfaces," International Journal of Machine Tools, **20**, pp.123-136.

[18] Choi, W., and Kurfess, T.R., 1999, "Dimensional measurement data analysis, Part 1: a zone fitting algorithm," Journal of Manufacturing Science and Engineering, **121**, pp. 238-245.

[19] Choi, W. and Kurfess, T.R., 1999, "Dimensional measurement data analysis, Part 2: a minimum zone evaluation," Journal of Manufacturing Science and Engineering, **121**, pp. 246-250.

[20] Wang, Y., 1992, "Minimum zone evaluation of form tolerances," Manufacturing Review, **5** (3), pp. 213-220.

[21] Etesami, F., and Qiao, H., 1990," Analysis of two-dimensional measurement data for automated inspection," Journal of Manufacturing Systems, **9**, pp. 21–34.

[22] Carr, K., and Ferreira, P., 1995, "Verification of form tolerances part I: Basic issues, flatness, and straightness," Precision Engineering, **17** (2), pp. 131-143.

[23] Qian, X., Robinson, M. D., and Ross, J., 2005, "Admissible transformation volume for part dimensional quality gauging," Computer-Aided Design, **37**(13), pp. 1335-1352.

[24] Smith, L., 2002, A tutorial on Principal Components Analysis, On the WWW, July. http://www.cs.otago.ac.nz/cosc453/student_tutorials/ principal_components.pdf.

[25] Allen, D. W., Harsch, A. F., and Machin, J. D., 1995, "Computer-Aided Marine Propeller Inspection Data Analysis," Naval Engineers Journal, **107**, pp. 33–40.

[26] Ye, P., Zhang, H.., Chen, K., and Wang, J., 2006, "The knot factor method and its applications in blade measurement," Aerospace Science and Technology, **10**(5), pp. 359-363.

[27] Kolda, T. G., Lewis, R. M., and Torcozn, V., 2003, "Optimization by Direct Search: New Perspective on Some Classical and Modern Methods," Society for Industrial and Applied Mathematics, **45**(3), pp. 385-482.

[28] THOME Praezision, 2009, CAPPS: Measuring Software for Coordinate Measuring Machines, On the WWW, October. URL http://www.thome-praezision.de/eng/.

[29] The touch probe learning center, 2011, Mechanical operation, On the WWW, May. URL http://www.geomet-cmm-software.com.

[30] Schuster, C.M., and Thoreson, R., 2003, Laser scanner helps define part profile, On the WWW, July. URL http://www.vision-systems.com.

[31] Itoh, K., and Ohno, Y., 1993, "A curve fitting algorithm for character fonts," Electronic Publishing, **6**(3), pp. 195-198.

[32] Nelder, J. A., and Mead, R., 1965, "A simplex method for function minimization," The Computer Journal, **7**, pp. 308-313.